

POLITECNICO DI TORINO

Master degree in Electronic Engineering

Master's degree thesis

**Electromagnetic and thermal  
modeling of passive radiative  
cooling for photovoltaic systems**



Supervisors:

Dr. Alberto TIBALDI

Prof. Federica CAPPELLUTI

Dr. Matteo CAGNONI

Candidate:

Pietro TESTA

April 2022

*To my family, friends, and  
Giorgia.*

I would like to thank my thesis supervisors Dr. Tibaldi, Prof. Cappeluti, Dr. Cagnoni, for their availability and assistance during the entire work.

# Summary

In recent years, the sharp rise in energy consumption and the growing concern about climate change have increased the demand for innovative technologies that can accelerate the path towards a sustainable future. The goal of reaching a greener economy can only be achieved by re-designing most of the traditional technologies and industrial processes, with the purpose of mitigating their environmental impact. Cooling systems are one of these technologies. They are the only relief against unstoppable global warming, yet they are energy-intensive and contribute to air pollution generating a climate feedback loop. In this context, the thesis work aims to investigate an alternative and greener technique, *i.e.*, daytime passive radiative cooling. Every body on Earth emits heat by radiation, whose spectral density depends on Planck's law and the emissivity of the object. For the typical temperatures found on Earth, the spectral density is concentrated in the *atmospheric transparency window*, *i.e.*,  $\lambda \simeq 8 \div 13 \mu\text{m}$ , where the atmosphere is almost transparent. Kirchhoff's law of thermal radiation ensures that absorptivity and emissivity spectra of a body coincide, hence all thermal radiation goes to outer space without any absorption from the atmosphere, leading to a cool-down of the material. In particular, the work examines the potential of such technology applied to photovoltaic systems. It is well known that part of the Sun radiation absorbed by solar cells is converted into heat instead of electricity, yielding typical operating temperatures of about  $50^\circ\text{C}$  or higher in terrestrial applications, under 1-sun illumination, with local variations. However, both efficiency and reliability of the photovoltaic system deteriorate at high temperatures, limiting in practice the annual energy yield and lifespan. Therefore, the goal is to study the application of the radiative cooler as heat sinks for the solar cell to maximize efficiency. To this aim, the development of an electromagnetic-thermal self-consistent model for simulating the performance of new materials based on radiative cooling technology and their impact on solar cell efficiency is proposed. The first part of the thesis focuses on the analysis of the theory underlying the radiative cooling mechanism and on the elaboration of a thermal model based on a steady-state heat flux balance equation. It evaluates the performance of the radiative cooler, *i.e.*, its temperature at equilibrium. Then, the development of a model that estimates the enhancement of the solar cell efficiency due to the radiative cooler is presented. More precisely, the device under test is composed of a radiative cooler below the solar cell based on crystalline semiconductors. The model is composed of two parts: a script based on the detailed-balance method presented by Shockley-Queisser for the computation of the power density produced by a photovoltaic cell at a certain temperature, and the above mentioned thermal model for the evaluation of the temperature of the entire structure. The second part of the work is dedicated to the development of an electromagnetic model for multi-layer analysis based on the transmission line technique. It evaluates the dielectric properties of stratified materials, such as the reflection coefficient. This

model provides the possibility of testing different nanostructures to find the right emissivity for radiative cooling capability. Finally, the complete simulation tool is obtained from the combination of the electromagnetic and thermal models.

# Table of contents

<b>Summary</b>	ii
<b>1 Introduction</b>	<b>1</b>
1.1 Electricity demand . . . . .	1
1.2 Solar spectra . . . . .	3
1.3 Photovoltaic effect . . . . .	5
1.4 Theory of solar cell: Shockley and Queisser . . . . .	8
1.4.0.1 Solar spectral photon flux . . . . .	9
1.4.1 Ultimate efficiency . . . . .	10
1.4.2 Detailed balance efficiency limit . . . . .	12
1.4.2.1 Solar generation current . . . . .	14
1.4.2.2 Recombination current . . . . .	14
1.4.2.3 JV characteristics . . . . .	16
1.4.2.4 Efficiency of a solar cell . . . . .	18
1.4.3 Loss mechanisms . . . . .	21
1.5 Effect of temperature on solar cells . . . . .	22
1.5.1 Thermalization process . . . . .	22
1.5.2 Performance degradation . . . . .	23
1.5.2.1 Open-circuit voltage . . . . .	24
1.5.2.2 Short-circuit current . . . . .	25
1.5.2.3 Efficiency . . . . .	26
1.5.3 Lifespan degradation . . . . .	27
1.6 Cooling of solar cells . . . . .	27
1.6.1 Active . . . . .	28
1.6.2 Passive . . . . .	28
1.6.2.1 Radiative cooling technique . . . . .	29
<b>2 The fundamentals of thermal radiation</b>	<b>30</b>
2.1 The heat transfer mechanisms . . . . .	30
2.2 Thermal radiation nature . . . . .	32
2.3 Black body . . . . .	34
2.3.1 Quantitative definition . . . . .	35
2.3.2 Black body as perfect emitter . . . . .	38
2.3.3 Isotropic emitter . . . . .	39
2.3.4 Uniform spectral emitter . . . . .	41
2.3.5 Effect of temperature on radiation . . . . .	41
2.4 Planck's law . . . . .	41
2.4.1 Solid angle . . . . .	42
2.4.2 Set up the heat transfer problem . . . . .	42
2.4.3 Projected area . . . . .	44
2.4.4 Spectral radiation intensity . . . . .	45

2.4.5	Black body hemispherical emissive power . . . . .	45
2.4.6	Planck's law . . . . .	46
2.5	Non-black body surface . . . . .	48
2.5.1	Emissivity . . . . .	49
2.5.1.1	Gray and diffuse surface . . . . .	49
2.5.1.2	Spectral directional emissivity . . . . .	50
2.5.1.3	Spectral hemispherical emissivity . . . . .	51
2.5.1.4	Directional total emissivity . . . . .	52
2.5.1.5	Hemispherical total emissivity . . . . .	52
2.5.2	Absorptivity . . . . .	53
2.5.2.1	Directional spectral absorptivity . . . . .	54
2.5.3	Kirchhoff's law . . . . .	55
<b>3</b>	<b>Radiative cooling</b>	<b>58</b>
3.1	Night-time radiative cooling . . . . .	58
3.1.1	Atmosphere power density . . . . .	59
3.1.2	Surface power density . . . . .	62
3.1.2.1	Black body thermal emitter . . . . .	63
3.1.2.2	Optimal selective thermal emitter . . . . .	64
3.1.2.3	Selective thermal emitter . . . . .	65
3.1.3	Comparison between emitters . . . . .	67
3.2	Day-time radiative cooling . . . . .	68
3.2.1	Solar power density . . . . .	69
<b>4</b>	<b>The impact of a radiative cooler on solar cell</b>	<b>70</b>
4.1	Thermal model . . . . .	70
4.1.1	Heat balance equation . . . . .	70
4.1.2	Electrical power density . . . . .	72
4.1.3	Radiated power density . . . . .	73
4.1.4	Convection and conduction power . . . . .	73
4.2	Results . . . . .	75
4.2.1	Vacuum . . . . .	75
4.2.1.1	Terrestrial environment . . . . .	75
4.2.1.2	Extraterrestrial environment . . . . .	77
4.2.2	Atmosphere . . . . .	78
4.2.2.1	Net cooling power . . . . .	78
4.2.2.2	Operating temperature . . . . .	79
4.2.2.3	Efficiency . . . . .	80
4.2.3	Towards realistic radiative coolers . . . . .	81
4.2.3.1	Emissivity of photonic structures . . . . .	81
4.2.3.2	Solar cell performance . . . . .	83
	<b>Conclusions</b>	<b>85</b>
	<b>Bibliography</b>	<b>87</b>

# Chapter 1

## Introduction

The world energy demand has been growing faster and faster over the years, while the employment of renewable energy has been expanding but not enough. Hence, it is essential to optimize the energy production system and research new technologies that provide the same service with lower energy consumption and less polluting. In this thesis, a new solution for improving the efficiency and the lifespan of solar cells will be treated. Specifically, in this chapter is analyzed the basic principle behind the solar power conversion process and the characterization of a solar cell through some figures of merit. Then, it is shown how high operating temperature can affect these parameters and how innovative technologies can passively act to improve them. Indeed, a small decrease in the solar cell temperature can lead to a significant increase in energy conversion.

### 1.1 Electricity demand

Climate change is strongly influenced by the energy sector. The production of energy accounts for two-thirds of the global emission of gases that have caused the increase of temperature of 1.1 °C compared to the pre-industrial age. Hence, the gradual elimination of coal and gas in this sector, the diffusion and integration of renewable energies, and higher energy efficiency are the fundamental steps to counteract the climate crisis and to support the inevitable growth of energy production. To this scope, the number of nations that have pledged to achieve net-zero emission (NZE) by 2050 continues to grow, which is in line with the framework set by the Paris Agreement in 2015. The common objective is to build a new energy economy based on efficiency, interconnection, and clean production of electric power. In this regard, the Covid-19 pandemic has shown the essential role of electricity in society. It sustained the sanitary system, vital services, and allow people to remain in contact and informed. Simultaneously, it highlighted the necessity to invest in renewable energies. After the first year of the Covid-19 crisis, the rebound of the economy required a 5% rise in global electricity production, half of which was met by fossil fuels [1].

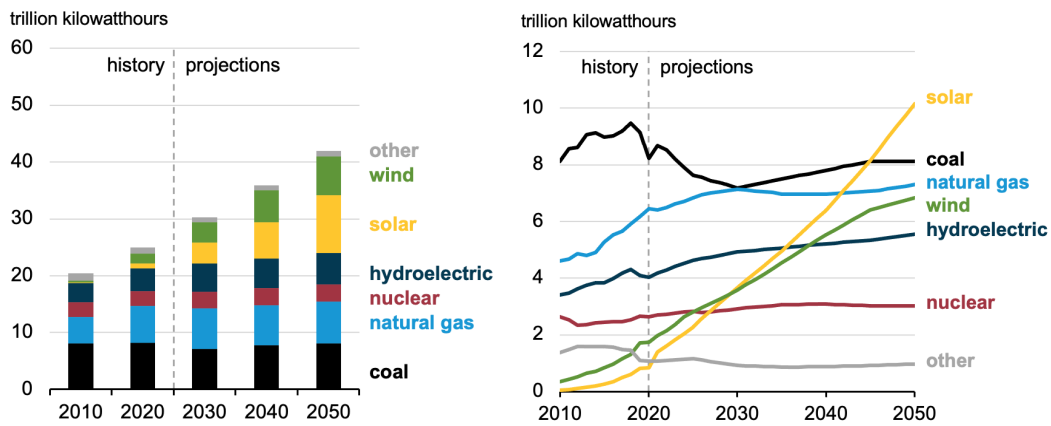


Figure 1.1: World net electricity generation by sources (IEO2021 [2])

The graphics in figure (1.1) show the relentless growth of electricity demand and the sources employed to support it. Since coal and gas are plentiful and inexpensive sources, they continue to be used for energy production in economies of developing countries, such as India and Africa. However, the exponential growth of renewable energies in the advanced economy leads to the containment of the CO<sub>2</sub> global emissions. In order to achieve a substantial reduction in the use of fossil fuels and their impact on climate change, it is essential to invest in clean energies such as solar power, wind power, hydroelectric power, and nuclear power. Improvement in energy efficiency is a fundamental actor in the transition towards a *low-carbon* economy (LCE). The technology innovation enables the reduction of renewable energies costs and the enhancement in energy production. In figure (1.2) is reported the potential growth of electricity demand in developing economies and emerging market. It is evident the impact of technological advancement in the generation of electric power. The energy-saving is almost 1700 TWh in developing

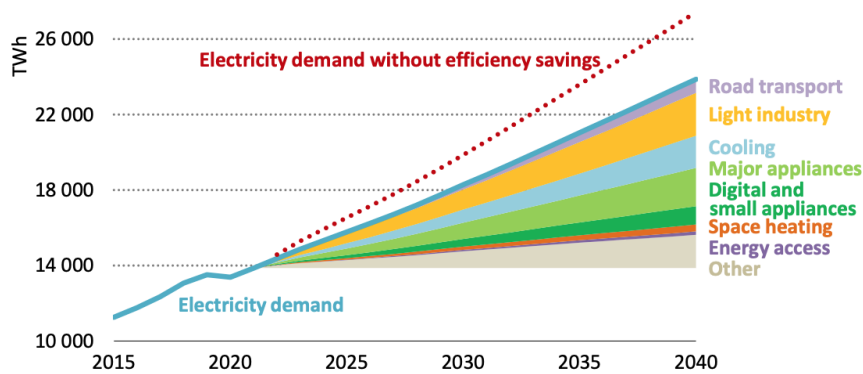


Figure 1.2: Drivers of electricity demand in emerging market and developing economies (WEO2020 [3])

economies, which corresponds to about 40% more than in advanced economies. In this context, this work aims to examine the conversion of solar power into electric power, and to find technology improvements to increase the efficiency of this process. In particular, the focus is on solar cells, which are optoelectronic devices that convert solar power into electrical power. Since this source is and will be one of the main actor in electric energy production, a small improvement in its efficiency leads to a significant increase of overall energy production.

## 1.2 Solar spectra

The sun sends every day an enormous amount of power to the Earth in the form of electromagnetic waves. The total power emitted is not composed of a single wavelength but many, indeed, for example, this fact allows people to see different colors. The solar spectral irradiance defines the power received from the Sun by a surface per unit area per unit of wavelength,  $\frac{W}{m^2nm}$ . This quantity is influenced by many atmospheric factors, then, it changes with respect to the condition in which is measured. The most significant difference is between the extraterrestrial and terrestrial spectrum since part of the light is absorbed and scattered by the atmosphere, attenuating the solar power. For example, most of the ultraviolet light is blocked by the atmosphere, only wavelengths from 315 to 400 nm (UVA) reaches the ground (Figure 1.3). It is fundamental to define a standard reference for the evaluation of solar cells' performance. The most significant parameter that affects the solar spectrum on Earth is the distance that the light has to travel through the atmosphere. Hence, the *air mass coefficient*(AM) was introduced to identify the solar spectrum employed in the evaluation of the solar cell performance. It is described as [4]:

$$AM(\theta) = \frac{L(\theta)}{L_0} \quad (1.2.1)$$

where  $L$  is the distance crossed by the sun radiation in the atmosphere, m, which depends on the polar angle,  $\theta$ ,  $L_0$  is the distance crossed by the sun radiation in the atmosphere at the zenith, m. Increasing the angle of incidence, the light is more attenuated since the optical path length is longer. There is an approximated version of (1.2.1), which is:

$$AM(\theta) \approx \frac{1}{\cos\theta} \quad (1.2.2)$$

where the only parameter necessary is the polar angle.

From figure (1.3), one can notice the presence of two different solar spectra: AM0

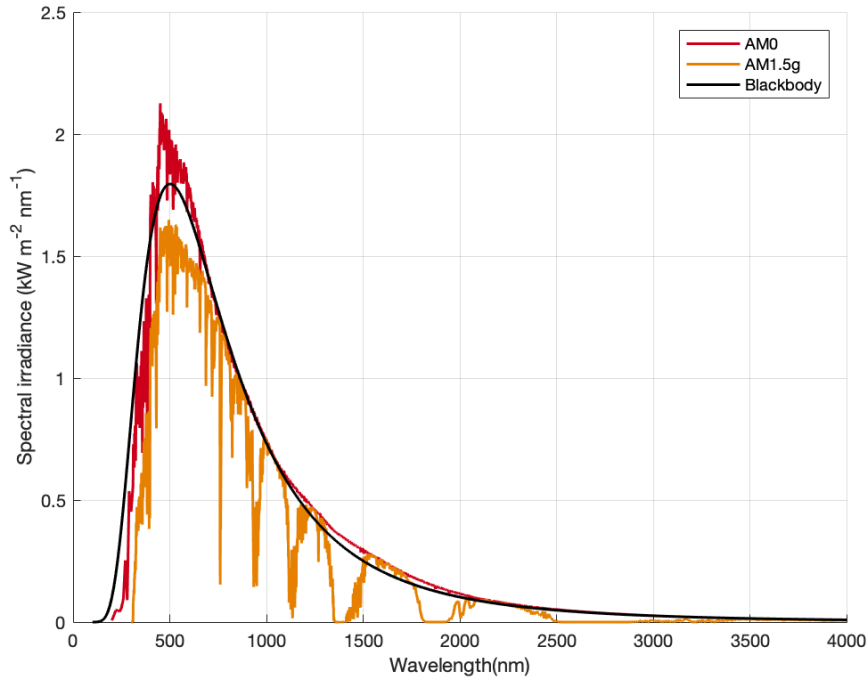


Figure 1.3: Solar spectral irradiance for different conditions

is the extraterrestrial spectrum<sup>1</sup>, AM1.5g is the terrestrial solar spectrum<sup>2</sup> for a polar angle of  $48.2^\circ$ . The data of AM0 and AM1.5g spectra are taken from the National Renewable Energy Laboratory(NREL) website, they are the reference spectra defined by the American Society for Testing and Materials (ASTM) [5, 6]. The extraterrestrial spectrum is measured just outside the atmosphere, near-Earth orbit, while the terrestrial spectrum at the ground. The solar irradiation is mainly condensed in the range of wavelength from 300 to 2500 nm with the maximum around the 500 nm.

The second thing that one can extrapolate from the above figure is the similarity between the AM0 spectrum and the one of the black body<sup>3</sup> at 5778 K, which is the temperature of the solar surface. This resemblance means that the sun emissivity is approximately isotropic. The AM0 is defined considering the distance between the earth and sun, the radius of the sun, and its surface power density [7]. Then,

<sup>1</sup>Zero stands for “zero atmospheres”

<sup>2</sup>The g stands for “Global spectrum”, it comprehends the direct and diffuse solar radiation and it is calculated for flat plate modules. Instead, the AM1.5d spectrum includes only the direct sun radiation and it is designed for solar concentration systems. The direct radiation is the ones that reach the ground without being scattered by the atmosphere

<sup>3</sup>It is an idealized object that absorbs and emits radiation in every direction and at any energy. The complete physical description of this object is reported in the Chapter 2 (Sec. 2.3).

the black body solar spectrum is calculated as follow [8]:

$$E_{BB}(T,\lambda) = I_{BB}(T,\lambda)\Omega_{Sun} \quad (1.2.3)$$

where  $I_{BB}$  is the spectral radiation intensity (Eq. 2.4.18),  $\Omega_{Sun}$  is the solid angle between a surface on Earth and the Sun and is expressed as:

$$\Omega_{Sun} = \pi \left( \frac{R_{Sun}}{AU - R_{earth}} \right)^2 \quad (1.2.4)$$

where  $R_{Sun}$  is the radius of Sun, km,  $AU$  is the astronomical unit, km,  $R_{earth}$  is the radius of Earth, km.

### 1.3 Photovoltaic effect

Here, a brief explanation of the conversion process behind single-junction solar cells (SJ) is given. A more exhaustive discussion of this topic is reported in [8]. Solar cells use the photovoltaic effect to convert solar power into electricity, which consists in the generation of electric current and voltage in a material exposed to light. To exploit this physical and chemical effect a semiconductor device is employed.

Semiconductors are materials characterized by a low energy gap, e.g., approximately 1.1 eV for silicon, and the possibility of engineering their electrical properties, such as conductivity. Now, consider a semiconductor at a temperature different from absolute zero and without the presence of external forces. In this condition, the semiconductor is in thermodynamic equilibrium, *i.e.*, there is a continuous generation and recombination of carriers. The electrons are thermally excited and jump into the conduction band leaving holes in the valance band. At the same time, excited electrons release their energy in form of heat or light and recombine with holes. Hence, the concentrations of holes,  $p$ , and electrons,  $n$ , in the two bands are constantly equal,  $n=p=n_i$ , where  $n_i$  is the intrinsic carrier

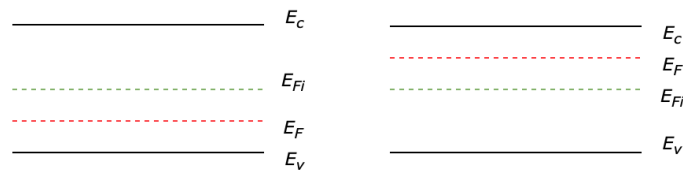


Figure 1.4: Band diagrams of a  $n$ -type and  $p$ -type semiconductors

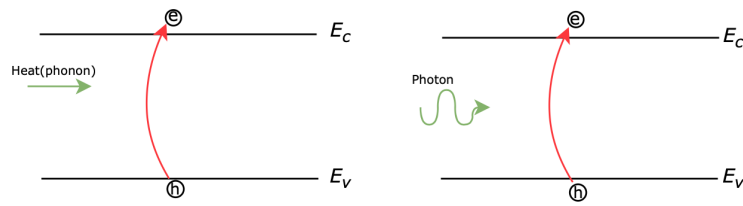


Figure 1.5: The most common generation processes in semiconductors. Left: Thermal generation Right: Photogeneration

density. The concentrations in a semiconductor at typical operating temperatures are small, then, the conductivity is many order of magnitude lower than that of metals, e.g., approximately  $0.31 \cdot 10^{-5} \frac{1}{\Omega \text{cm}}$  for silicon. To overcome this problem, impurities (dopants) are introduced in the silicon lattice leading to an addition of positive or negative free carriers, this is the so-called *doping* process. Now, the number of charge carriers is determined by the number of dopants, allowing the electrical properties of the material to be controlled. The semiconductors with high concentrations of electrons and holes are called *n*-type and *p*-type respectively, and the majority and minority carriers are indicated with  $n_n/p_p$  and  $p_n/n_p$ . The Fermi levels of *extrinsic* semiconductors move from the band gap center towards the conduction or valance band, depending on the concentration of carriers (Figure 1.4). For example, in *n*-type semiconductor, the Fermi level,  $E_F$ , is closer to the conduction band due to the high concentration of electrons.

Now, consider a semiconductor exposed to light. The photons incident on it with energy equal or greater than band gap,  $E \geq E_g$ , are absorbed and deliver their energy to electrons that jump into the conduction band. This process is called *photogeneration* and occurs alongside the thermal generation (Figure 1.6).

The electrons in the conduction band are free to move. Then, a current can be generated by connecting the semiconductor to an external circuit and imposing a potential difference. But to convert solar power into electric power, the semiconductor should behave like a generator, *i.e.*, it generates an internal electric field to move the electron and transport their power to an external load. This can be done by exploiting a *pn* junction. When *p*-type and *n*-type semiconductors are joined, the majority carriers diffuse in the other side of the junction leaving fixed charges (Left Figure 1.6). The negative ions in the *p*-region and positive ions in the *n*-region generate an electric field at the junction, which removes the free carriers forming the *depletion* region. Moreover, it generates the built-in potential,  $qV_{bi}$ , which works as a potential barrier for the fluxes of majority carriers (Left Figure 1.6). Now, consider exposing the *pn* junction connected to a load to light.

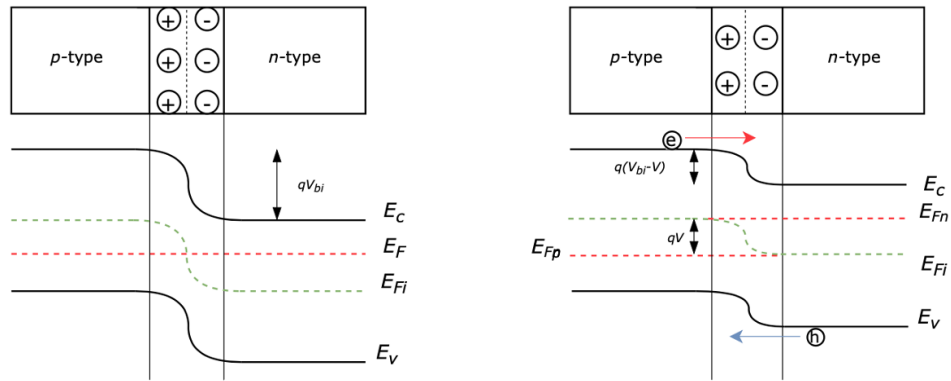


Figure 1.6: Left:  $pn$  junction in thermal equilibrium. Right:  $pn$  junction exposed to the Sun.

The absorbed incident photons generate e-h pairs along the device. The majority carrier cannot diffuse in the other region due to the potential barrier. Instead, the minority carriers are moved by the electric field generated by the fixed carrier from one side to the other (Right Figure 1.6). Then, these carriers are collected to the metal contacts, and their power is delivered to the external load. In this condition, the  $pn$  junction is *out of equilibrium* because the fluxes of carriers between the regions are not balanced. Hence, an internal voltage is generated to lower the potential barrier and restore the equilibrium. In other words, the junction is now *self forward-biased*, which means that the built-in potential is reduced of the difference between the two quasi-Fermi levels,  $qV = E_{Fn} - E_{Fp}$ .

Figure (1.7) shows the JV-characteristics of a  $pn$  junction forward-biased and under illumination, and the current-voltage convention employed. In the first case, the junction works as a diode, *i.e.*, it is controlled by an external voltage. In the latter case, the current has a negative sign since it goes from the junction to the load. This is the only condition in which the  $pn$  junction works as a generator, which means that it provides power to the external load. It is interesting to notice two particular working points of the solar cell exposed to light. First, when the  $pn$  junction is not connected to an external load, the current is zero and the voltage reaches the maximum value, it is called the open-circuit voltage,  $V = V_{OC}$ . All the e-h pairs generated remain in the device, so the potential barrier is strongly reduced to balance the fluxes of carriers. Second, when the device is short-circuited, all the e-h pairs photogenerated deliver their power to the load forming the so-called short circuit current,  $J_{sc}$ . In both working conditions, the power generated by the photodiode is zero.

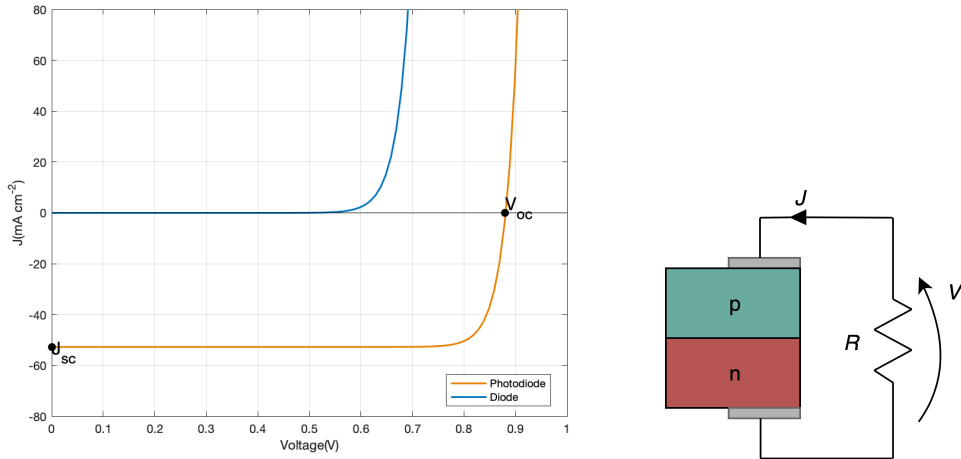


Figure 1.7: Left: JV characteristics of a diode and a photodiode. Right:  $pn$  junction connected to an external load

The JV characteristics are computed by the formula:

$$J = J_s(e^{\frac{qV}{kT}} - 1) - J_{ph} \quad (1.3.1)$$

where  $J_s$  is the saturation current density,  $\frac{A}{\text{cm}^2}$ ,  $\frac{q}{kT}$  is the thermal voltage,  $V$ ,  $J_{ph}$  is the photocurrent density,  $\frac{A}{\text{cm}^2}$ .

The JV characteristics reported in figure (1.7) are calculated for a silicon  $pn$  junction with saturation current equal to  $2 \cdot 10^{-13} \frac{A}{\text{cm}^2}$  [9], thermal voltage equal to 0.026 V, and the photocurrent is computed by the equation (1.4.26).

## 1.4 Theory of solar cell: Shockley and Queisser

The very complex physics behind the  $pn$  junction and the photocurrent generation does not allow the definition of the maximum conversion efficiency of a single junction solar cell. Then, W. Shockley and H. J. Queisser in the article “Detailed Balance Limit of Efficiency of  $pn$  Junction Solar Cells” proposed a different approach to compute the maximum efficiency [10]. The idea behind this work is to study an idealized  $pn$  junction from a thermodynamic point of view. Hence, all the non-radiative processes are neglected, and only the radiative recombination process is considered. In this view, it is possible to compute the theoretical upper limit of the single-junction solar cell efficiency at a certain temperature in terrestrial and extraterrestrial environments. This section is dedicated to the characterization of the solar cell by introducing a similar model to the one developed

in the Shockley-Queisser paper.

### 1.4.0.1 Solar spectral photon flux

It is useful for the computation of solar cell efficiency to employ the spectral photon flux instead of the spectral irradiance.

The spectral photon is defined as the number of photons per unit area, per unit time, per unit energy:

$$\phi_E(E) = \frac{d\text{photons number}}{dE dA dt} \quad (1.4.1)$$

where the subscripts “E” indicates that is a spectral quantity. Then, it can be rewritten as:

$$\phi_E(E) = \frac{d\text{photons power}}{dA d\lambda} \left| \frac{d\lambda}{dE} \right| \frac{\frac{d\text{photons number}}{dt}}{d\text{photons power}} \quad (1.4.2)$$

where the first term is a spectral power density and corresponds to the solar spectral irradiance,  $\frac{W}{m^2_{nm}}$ , and the last one is equal to the inverse of the photon energy  $\frac{1}{E}$ ,  $\frac{1}{J}$ . The center term is computed by recalling the Planck relation (Eq. 2.2.10), so:

$$\left| \frac{d\lambda}{dE} \right| = \left| \frac{d}{dE} \left( \frac{hc}{E} \right) \right| = \frac{hc}{E^2} \quad (1.4.3)$$

substituting this expression in the (1.4.2), the solar photon flux per unit energy is computed as:

$$\phi_E^i(E) = AM \frac{hc}{E^2} \frac{1}{E} = AM \frac{hc}{E^3} \quad (1.4.4)$$

its unit is  $\frac{1}{m^2 s J}$ .

where  $AM$  is the general term to indicate spectral irradiance. It corresponds to the  $AM1.5_g$  spectrum in the terrestrial case, and to the  $AM0$  spectrum in the extraterrestrial case. Figure (1.8) depicts the variation of  $\phi_E^i$  with respect to the energy. This representation allows an immediate relation with the energy gap of the solar cell. For example, if it is assumed that each photon with energy greater than the energy gap,  $E \geq E_g$ , is absorbed, then, one could think that silicon(Si) solar cells can generate more electrical power than gallium arsenide(GaAs) solar cells since it absorbs more photons.

Now, it is possible to compute the total power density received from the Sun as:

$$P_{tot} = \int_0^{\infty} \phi_E^i(E) E dE \quad (1.4.5)$$

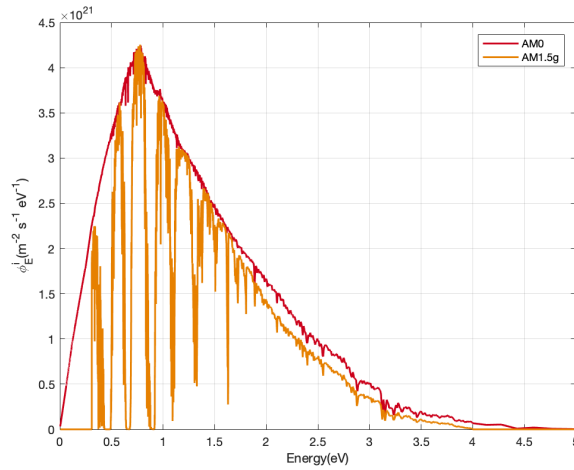


Figure 1.8: The solar photon flux per unit of energy

The number of photons at each energy is multiplied by the energy itself to get the power contribution and it is summed by the integral. It corresponds to the total power available from the sun per square meter. Evaluating this integral using the data of NREL terrestrial solar spectrum,  $AM1.5_g$ , it is obtained:

$$P_{tot} = 1002 \frac{\text{W}}{\text{m}^2} \quad (1.4.6)$$

this value is usually normalize to  $1 \frac{\text{kW}}{\text{m}^2}$ . The total solar power outside the atmosphere,  $AM0$ , is equal to:

$$P_{tot} = 1367 \frac{\text{W}}{\text{m}^2} \quad (1.4.7)$$

### 1.4.1 Ultimate efficiency

A first theoretical efficiency limit can be defined by studying an ideal experiment. Consider a short-circuited solar cell that absorbs all the photons with energy greater than the semiconductor band gap. Then, the absorptivity is a step function defined as:

$$\alpha(E, E_g) := \begin{cases} 1 & E_g \leq E \\ 0 & E_g > E \end{cases} \quad (1.4.8)$$

This quantity defines the power absorbed by the solar cell at each energy. The solar cell is assumed to be at absolute zero,  $T = 0 \text{ K}$ . The incident photons come from every direction and have different energies. Each of them generates an e-h pair. The excess photon energy is neglected, supposing that it is dissipated through some means maintaining the temperature at absolute zero. This implies

that the mobility of the carriers tends to infinity, so their collection is independent from the position in which are generated. To be clear, there is no energy, such as heat, provided to the electrons to jump in the conduction bands except for the one that receives from solar radiation. Finally, it is assumed that neither radiative nor non-radiative recombination processes occur, all the e-h pairs pass through the short circuits and recombine at the metal plates. Hence, when the solar cell is exposed to the Sun, all the generated e-h pairs contribute to the electrical power. The power density absorbed from the Sun is calculated as:

$$P_{ult} = \int_0^{\infty} \alpha(E, E_g) \phi_E^i(E) E_g dE \quad (1.4.9)$$

where  $E_g$  is the energy gap of the solar cell, J. In this case, since it is assumed that the photons with energy greater than the energy gap are considered to have energy  $E_g$ , the solar photon flux is multiplied by  $E_g$ . The excess power,  $E - E_g$ , is not taken into account. Now, the (1.4.9) can be rewritten as:

$$P_{ult} = E_g \int_{E_g}^{\infty} \phi_E^i(E) dE = E_g \phi_{E_g}^i \quad (1.4.10)$$

where  $\phi_{E_g}^i$  is the number of photons with energy greater than the energy gap,  $\frac{1}{m^2s}$ . Finally, it is possible to compute the ultimate efficiency as:

$$\eta_{ult}(E_g) = \frac{P_{ult}(E_g)}{P_{tot}} = \frac{E_g \phi_{E_g}^i}{P_{tot}} \quad (1.4.11)$$

where  $\eta_{ult}$  is normally expressed in percentage.

Figure (1.9) shows the dependence of the efficiency on the energy gap. In the terrestrial case, the maximum value is 49.1% and is reached for a solar cell with  $E_g = 1.12\text{eV}$ , which corresponds to the one of silicon. In the extraterrestrial case, the maximum value is 44% and it is reached for an solar cell with  $E_g = 1\text{eV}$ .

Of course, the power generated by a solar cell in space is greater than the one of a solar cell on the ground, but the same occurs for the available total power. Then, the extraterrestrial efficiency is greater than the terrestrial one only from 2.25 to 3.9 eV. This difference is due to the ultraviolet light, which is present in the  $AM0$  spectrum but not in the  $AM1.5_g$  spectrum, where it is mostly blocked by the atmosphere and so does not contribute to the current generation.

It is interesting to notice that the efficiency of a single-junction solar cell cannot reach higher values because the excess power is a significant intrinsic loss. The

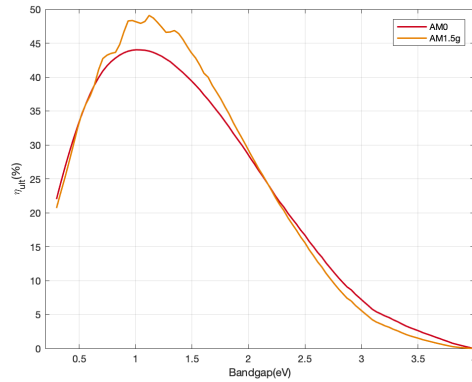


Figure 1.9: The ultimate efficiency with respect to the energy gap

other loss is due to the sub-bandgap photons. On the basis of the initial assumptions, it is important to interpret this result in the right way: these values are not reachable, and so the scope of this parameter is to show that it is impossible to ever have higher efficiencies or solar cells describable by the SQ model.

### 1.4.2 Detailed balance efficiency limit

The ultimate efficiency is computed for a photovoltaic cell that works in ideal conditions at 0 K. Then, it is useful to define an efficiency in a more realistic condition, *i.e.*, *detailed balance efficiency*.

To this scope, consider a  $pn$  junction at a temperature  $T$ , different from 0 K, connected through a resistance and constantly exposed to solar radiation (Figure 1.10). Furthermore, it has a mirror on the rear that is a perfect reflector. This configuration slightly increases the efficiency of the solar cell since the radiative losses into one of the two hemispheres are eliminated [11]. In other words, the radiation emitted towards the lower hemisphere is reflected and then absorbed by the structure, dual-pass cell.

In this view, the processes that take place are:

- radiative generation: generation of e-h pairs due to solar incident photons
- radiative recombination: elimination of an e-h pair and the emission of a photon
- non-radiative generation: thermal generation of e-h pairs
- non-radiative recombination: elimination of an e-h pairs through the emission of phonons

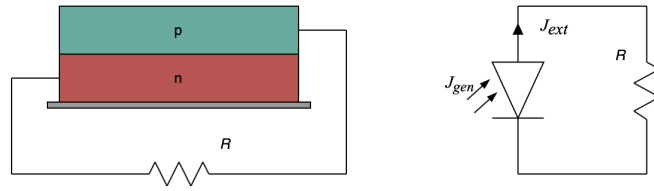


Figure 1.10: Left: the  $pn$  junction with mirror on the rear connected to an external resistance. Right: the equivalent circuit.

- current density generation due to the extraction of electrons from n-type region and holes from p-type region, thanks to the external resistance that connects the two regions

In order to calculate the electrical power produced by the solar cell, it is necessary to find the *steady state current-voltage relationship* through the balance equation. The sum of all the processes at steady state must be equal to zero. Furthermore, each process is characterized as current density, such as the solar generation current is equal to the solar photon flux multiplied by the electron charge. This allows to synthesize the five statements as [10, 12]:

$$J_{gen} - J_r(V) + J_{nr}(0) - J_{nr}(V) - J_{ext} = 0 \quad (1.4.12)$$

where  $J_{gen}$  is the maximum photocurrent density,  $J_r$  is the radiative recombination current,  $J_{nr}(0)$  is the non-radiative generation current density,  $J_{nr}(V)$  is the non-radiative recombination current density, and  $J_{ext}$  is the external current. They are all current density, so their measurement unit is  $\frac{A}{m^2}$ . The voltage,  $V$ , corresponds to the quasi-Fermi levels splitting due to the optics generation of e-h pairs. Then, it is different from zero when the junction is out of equilibrium, exposed to the sun light. Indeed, the non-radiative recombination and generation currents are indicated with the same subscripts since they are identical at equilibrium,  $V = 0$  V. It is assumed that the mobility of the carrier is infinite, as in the computation of the ultimate efficiency.

The external current is obtained from the equation (1.4.12):

$$J_{ext} = J_{gen} - J_r(0) + [J_r(0) - J_r(V) + J_{nr}(0) - J_{nr}(V)] \quad (1.4.13)$$

where  $J_r(0)$  is the radiative recombination current at equilibrium,  $\frac{A}{m^2}$ . It is important to notice two things. First, the equation (1.4.12) is written using the circuit generator convention, i.e., the solar cell works as a power source connected to a load (Right figure 1.10). Second, the external current density is a part of the

optical current generated by solar radiation and it is the only observable electric current of the cell.

The idea is to identify an efficiency upper limit for solar cells based on crystalline semiconductors but technology independent. Then, the detailed balance limit is computed neglecting the non-radiative recombination processes, which are described with very complex models, moreover, some of them are technology-dependent, such as Shockley-Read-Hall recombination (SRH).

Under these assumptions, the equation (1.4.12) becomes:

$$J_{ext} = J_{gen} - J_r(0) - J_{rec} \quad (1.4.14)$$

where:

$$J_{rec} = J_r(V) - J_r(0) \quad (1.4.15)$$

Now, the focus is on the meaning and evaluation of the generation and recombination terms to find the JV characteristic.

#### 1.4.2.1 Solar generation current

The solar generation current is the current that the solar cell would generate if the recombination processes do not occur, that is, each photon absorbed provides the energy to an electron that jumps in the conduction band and contributes to the electric current of the external circuit. Assuming, as before, that each photon with energy greater than the energy gap is absorbed, then:

$$J_{gen}(E_g) = q \int_0^\infty \alpha(E, E_g) \phi_E^i(E) dE = q \phi_{E_g} \quad (1.4.16)$$

where  $q$  is the electron charge:

$$q = 1.602\,176\,634 \cdot 10^{-19} \text{ C} \quad (1.4.17)$$

#### 1.4.2.2 Recombination current

To evaluate the efficiency of a solar cell is fundamental to consider the recombination processes, which reduce the number of electrons that contribute to the external current. As mentioned above, the only loss mechanism considered is the *radiative* recombination. Since the cell temperature is different from absolute zero, it emits radiation (Eq. 2.1.2). To do this, the electrons in the conduction band

jump back to the valance band releasing their energy in the form of an electromagnetic waves. At this point, the idea of Shockley-Queisser is not to focus on the solar cell and study the complex recombination processes, but to consider the entire system from a thermodynamic point of view. In these conditions, it is possible to apply the *detailed balance principle* to evaluate the radiative recombination rate of a material [13]. The problem can be divided into two parts: first, the evaluation of the photon flux at equilibrium condition and after at non-equilibrium condition, that is, in a dark room and exposed to the Sun respectively. To this scope, a conceptual experiment is put up by Shockley-Queisser to quantify the recombination rate.

Consider a open-circuited  $pn$  junction, no current flows in it, surrounded by a black body. The two objects exchange energy through heat radiation and the system is at thermal-radiative equilibrium, *i.e.*, both have the same temperature  $T$ . Then, it is possible to determine the photon flux per unit energy of a black body as in the case of the solar power, so:

$$\phi_E(E) = \frac{d\text{photons power}}{dA d\nu} \bigg|_{dE} \bigg|_{\frac{d\text{photons number}}{dt}} \frac{d\nu}{d\text{photons power}} \quad (1.4.18)$$

recalling the energy expression of the Plank's law (Eq. 2.4.14) and integrating it with respect to the hemisphere (Eq. 2.4.8), the spectral hemispherical photon flux is obtained:

$$\phi_E^e(E, T) = \frac{2\pi}{h^3 c^2} \frac{E^2}{e^{\frac{E}{k_B T}} - 1} \quad (1.4.19)$$

its unit is  $\frac{1}{\text{m}^2 \text{s J}}$ .

Since the junction emits only in one hemisphere, an hemispherical quantity is employed to evaluate the recombination current of the solar cell at equilibrium, which is defined as:

$$J_{r,0}(E_g, T) = q \int_0^\infty \alpha(E, E_g) \phi_E^e(E, T) dE \quad (1.4.20)$$

its unit is  $\frac{\text{W}}{\text{sr m}^2 \text{J}}$ .

At this point, it is possible to compute the recombination current when the solar cell is exposed to the Sun, *i.e.*, out of equilibrium. The radiative recombination is directly proportional to the product of holes and electrons densities. Then, the equation (1.4.15) can be generalized according to this assumption [10]:

$$J_{r,V}(E_g, T, V) = J_{r,0}(E_g, T) \left( \frac{np}{n_i^2} \right) \quad (1.4.21)$$

When the solar cell is not exposed to the sun radiation, at thermal equilibrium, the mass action law ensures  $n_i^2 = np$ , and so this current is equal to  $J_{r,0}$ . Recalling the Shockley's relations:

$$\begin{aligned} n &= n_i e^{\frac{E_{Fn} - E_{Fi}}{k_B T}} \\ p &= n_i e^{\frac{E_{Fi} - E_{Fp}}{k_B T}} \end{aligned} \quad (1.4.22)$$

where  $E_{Fn}$  and  $E_{Fp}$  are the Fermi level in a n-type and p-type semiconductors,  $J$ ,  $E_{Fi}$  is the Fermi level in a intrinsic semiconductor,  $J$ . Then, it is possible to write the product of holes and electrons concentrations as:

$$np = n_i^2 \left( e^{\frac{E_{Fn} - E_{Fp}}{k_B T}} - 1 \right) = n_i^2 e^{\frac{qV}{k_B T}} = n_i^2 e^{\frac{V}{V_T}} \quad (1.4.23)$$

where  $V$  is a voltage caused by the splitting between the two quasi-Fermi levels,  $V$ , and  $V_T$  is the Boltzmann thermal voltage, whose expression is:

$$V_T = \frac{k_B T}{q} \quad (1.4.24)$$

Out of equilibrium, the  $pn$  junction tries to eliminate the e-h pairs generated by the solar radiation by increasing the emission of photons. Now, substituting the equation (1.4.23) and (1.4.21) in the (1.4.15), it becomes:

$$J_{rec}(E_g, T, V) = J_{r,0}(E_g, T) \left( e^{\frac{V}{V_T}} - 1 \right) \quad (1.4.25)$$

it is interesting to notice that this expression is very similar to the Shockley diode equation, but it has the opposite sign since the solar cell generates a current as a battery does, then, it is used the *generator convection* (Right figure 1.10).

### 1.4.2.3 JV characteristics

Finally, it is possible to trace the current-voltage characteristic of a solar cell with an energy gap  $E_g$  at the temperature  $T$ , the expression is:

$$J_{ext}(E_g, T, V) = J_{gen}(E_g) - J_{r,0}(E_g, T) - J_{rec}(E_g, T, V) \quad (1.4.26)$$

Figure (1.11), it is possible to extrapolate two figures of merit that are useful to describe and compare solar cells. First, the solar cell is in short-circuit condition,  $R \rightarrow 0$ , the voltage internally generated is equal to zero. Hence, the solar generation current is equal to the external current, in this case, it is called the

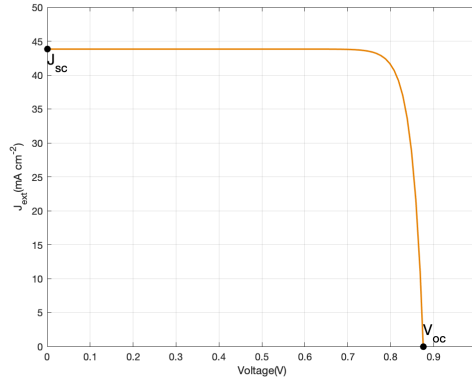


Figure 1.11: The JV characteristics of solar cells with  $E_g = 1.12$  eV at 300 K in terrestrial environment

*short-circuit current* and its expression is:

$$J_{SC} = J_{ext}|_{V=0} = J_{gen} - J_{r,0}(E_g, T) \quad (1.4.27)$$

It is possible to neglect the equilibrium recombination current density [12] and approximate this expression as:

$$J_{SC} \approx J_{gen} \quad (1.4.28)$$

Second, the solar cell is in open circuit configuration,  $R \rightarrow \infty$ , which implies that the current flowing through it is zero. At the steady state condition, the solar cell has to emit the same power that it absorbs from the Sun. Therefore, the maximum value of voltage is reached and it is called the *open-circuit voltage*. It is computed imposing the equation (1.4.26) equal to zero and  $V = V_{OC}$ , so:

$$0 = J_{gen}(E_g) - J_{r,0} - J_{rec}(E_g, T) = J_{gen}(E_g) - J_{r,0}(E_g, T)e^{\frac{V_{OC}}{V_T}} \quad (1.4.29)$$

Then:

$$V_{OC}(E_g, T) = V_T \ln \left( \frac{J_{gen}(E_g)}{J_{r,0}(E_g, T)} \right) \quad (1.4.30)$$

It is useful to analyze the variation of these two terms with respect to the energy gap (Figure 1.12). The short-circuit current monotonously decreases with the increase of the energy gap since the number of photons absorbed reduces.

The above figure shows the comparison between the open-circuit voltage and the band gap potential,  $\frac{E_g}{q}$ . It is interesting to notice that even if the short-circuit

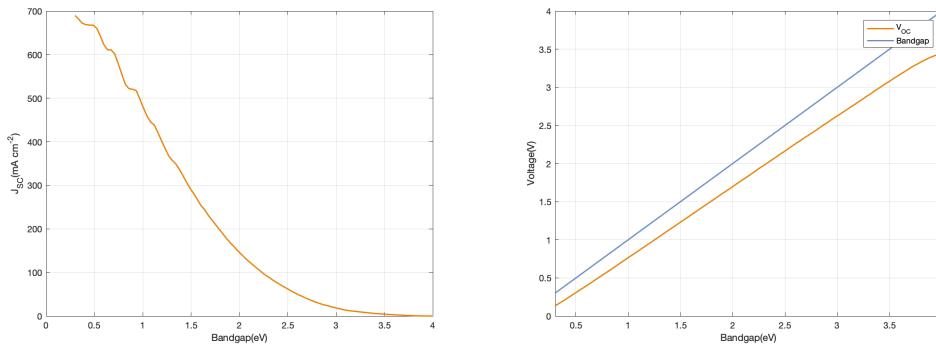


Figure 1.12: Left: the short-circuit current density with respect to the energy gap. Right: the comparison between the band gap potential and the open-circuit voltage with respect the energy gap for  $T=300$  K (terrestrial environment)

current decreases the open-circuit voltage has the opposite behavior. The recombination current reduces with a higher energy gap, then  $V_{OC}$  has to increase to recombine all the e-h pairs generated by the solar radiation. Although the open-circuit voltage constantly grows up, its slope is lower in respect of the band gap potential. This behavior is caused by the reduction of the carrier density in the bands at higher energy gaps, so the quasi-Fermi level move towards the intrinsic Fermi level [12].

#### 1.4.2.4 Efficiency of a solar cell

The power density generated by the solar cell can be easily computed by the circuit formula:

$$P = JV \quad (1.4.31)$$

its unit is  $\frac{W}{m^2}$ .

The solar cell is a generator that provides energy to an external load, which fixes the working point of the cell. The first thing to notice is that the short-circuit current and the open-circuit voltage are non-working points since the power generated in these operating conditions is zero. Therefore, it is necessary to compute the optimal load that forces the cell to work at the *maximum power point* (MPP), it is defined as:

$$R_{MPP} = \frac{V_{MPP}}{AJ_{MPP}} \quad (1.4.32)$$

its units is  $\Omega$ .

Then, the maximum power density produced by a solar cell is evaluated finding the maximum power point voltage and then substituting it in the equation (1.4.26) to compute the maximum power current density. Rewriting the equation that defines

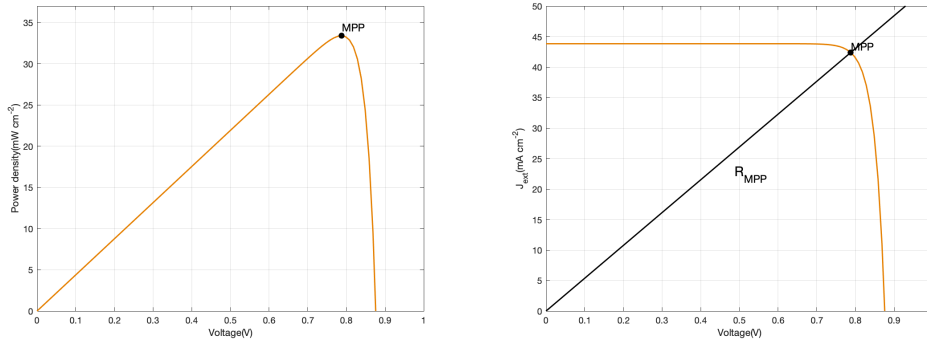


Figure 1.13: Left: The electric power of solar cells with respect to the voltage. Right: Graphical representation of the optimal load. (solar cell characteristics:  $E_g = 1.12$  eV,  $T = 300$  K, terrestrial environment)

the open-circuit voltage (1.4.29), it is possible to calculate the generation current density as:

$$J_{gen}(E_g) = J_{r,0}(E_g, T) e^{\frac{V_{OC}}{V_T}} \quad (1.4.33)$$

substituting it in the equation (1.4.26):

$$J_{ext}(E_g, T, V) = J_{r,0}(E_g, T) e^{\frac{V_{OC}}{V_T}} - J_{r,0}(E_g, T) - J_{r,0}(E_g, T) \left( e^{\frac{V}{V_T}} - 1 \right) \quad (1.4.34)$$

Then, the current is plugged in the power density equation:

$$P = J_{ext}(E_g, T, V) V = J_{rec,0}(E_g, T) \left( V e^{\frac{V_{OC}}{V_T}} - V e^{\frac{V}{V_T}} \right) \quad (1.4.35)$$

the maximum power point voltage can be computed by deriving the previous equation with respect to the voltage and searching for which value of  $V$  the equation is equal to zero, so:

$$\frac{\partial P}{\partial V} = J_{ext}(E_g, T, V) V = J_{rec,0}(E_g, T) \left( e^{\frac{V_{OC}}{V_T}} - e^{\frac{V}{V_T}} - \frac{V}{V_T} e^{\frac{V}{V_T}} \right) = 0 \quad (1.4.36)$$

Rewriting it:

$$e^{\frac{V_{MPP}}{V_T}} \left( 1 + \frac{V_{MPP}}{V_T} \right) = e^{\frac{V_{OC}}{V_T}} \quad (1.4.37)$$

Once maximum power point voltage is obtained, it is possible to compute the maximum power point current density plugging the  $V_{MPP}$  in the equation (1.4.34). Finally, the maximum power density is evaluated as:

$$P_{MPP}(E_g, T) = J_{MPP}(E_g, T) V_{MPP}(E_g, T) \quad (1.4.38)$$

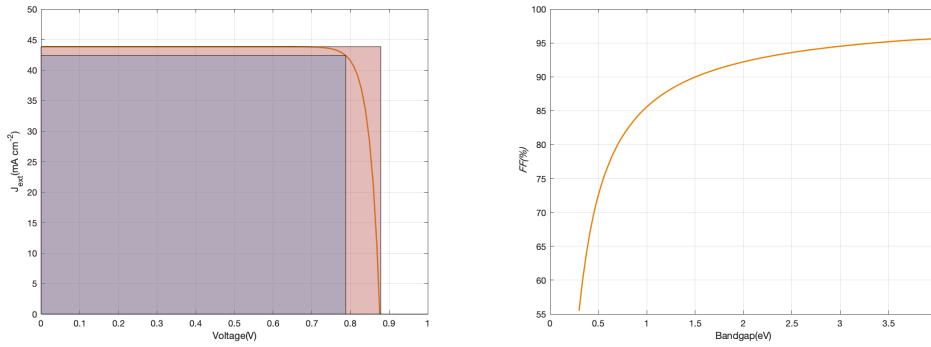


Figure 1.14: Left: Fill factor a ratio for solar cell with  $E_g = 1.12 \text{ eV}$ . Right: Fill factor with respect to the band gap (  $T = 300 \text{ K}$ , terrestrial environment)

It is the useful power. It is interesting to notice that the maximum power point is reached for a voltage and current values lower than  $V_{oc}$  and  $J_{sc}$ . Now, it is possible to introduce another solar cell figure of merit, which is the *fill factor*. It is defined as:

$$FF(Eg, T) = \frac{V_{MPP}(Eg, T) J_{MPP}(Eg, T)}{V_{OC}(Eg, T) J_{SC}(Eg)} \quad (1.4.39)$$

The  $V_{OC}$  and  $J_{SC}$  are the maximum current and the maximum voltage respectively, but the power generated from the solar cell is zero in both these points. The fill factor measures the quality of the solar cell. It compares the maximum power to the theoretical power. Graphically, it corresponds to the ratio between the two areas representing the powers (Left figure 1.14). In the right figure, one can note that the fill factor increases with the band gap since the *rounded* part of the JV curve occupy less area at higher voltages .

Now, the *detailed balance efficiency* is evaluated as:

$$\eta(Eg, T) = \frac{P_{MPP}(Eg, T)}{P_{tot}} \quad (1.4.40)$$

This parameter is fundamental to evaluate the impact of the radiative cooler on a solar cell's useful power. Figure (1.15) shows the efficiencies of a solar cell in terrestrial and extraterrestrial environments. In the terrestrial case, the maximum efficiency is reached for materials with an energy gap of around  $1.35 \div 1.5 \text{ eV}$ . In particular, the maximum value for a solar cell at  $300 \text{ K}$  is  $33\%$ . In the extraterrestrial case, the maximum efficiency is  $30.5\%$ , it is reached for an energy gap of about  $1.24 \text{ eV}$ . This efficiency limit for a single-junction solar cell is computed assuming that all the incident photons with  $E \geq E_g$  are absorbed and each one generates e-h pair, and the only recombination process is the radiative one.

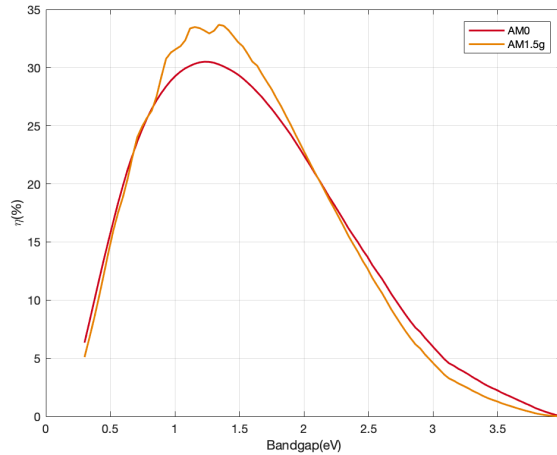


Figure 1.15: Efficiency of solar cells at 300 K

### 1.4.3 Loss mechanisms

Here, the *intrinsic* loss mechanisms present in a single-junction solar cell are examined. They occur independently from the technology and the working environment.

Since the radiative recombination reduces the number of photon that contributes to the electricity, it corresponds to a loss of power. The electrons from the conduction bands jumps back in the valance band releasing a quantity of energy equal to the band gap,  $E_g$ . Then, the radiative recombination loss for a solar cell working at its maximum power point can be computed as:

$$P_{rec}(E_g, T, V) = E_g \int_{E_g}^{\infty} \phi_E^e(E, T) e^{\frac{V_{MPP}}{VT}} dE \quad (1.4.41)$$

The power incident on the solar cell from the Sun is not completely absorbed *i.e.*, the sub-bandgap photons are reflected or transmitted. It is possible to evaluate this loss as:

$$P_{sub}(E) = \int_0^{E_g} E \phi_E^i(E) dE \quad (1.4.42)$$

its unit is  $\frac{W}{m^2}$ .

Part of the absorbed power is converted into heat through the *thermalization process*, which occurs for absorbed photons with energy higher than the energy gap. Then, it corresponds to a loss of useful power and it is computed as:

$$P_{th}(E) = \int_{E_g}^{\infty} (E - E_g) \phi_E^i(E) dE \quad (1.4.43)$$

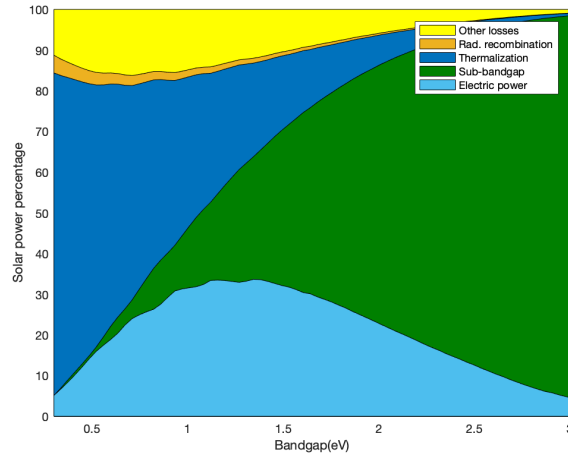


Figure 1.16: Decomposition of the total solar power,  $P_{tot}$ , incident on a solar cell at temperature of 300 K

its unit is  $\frac{\text{W}}{\text{m}^2}$ .

These are the main losses of the solar cell, as one can see in the figure (1.16). The thermalization is dominant for lower energy gaps since the number of photons absorbed with  $E > E_g$  is significant. At higher energies, most of the solar spectrum is reflected or transmitted leading to an increase of the sub-bandgap loss. The yellow portion of the plot takes into account the Boltzmann and Carnot losses, which are connected to the increase of entropy and thermodynamics laws [14].

## 1.5 Effect of temperature on solar cells

The solar cell is able to collect the solar energy and convert it into electricity. During this process part of the absorbed power dissipates into heat leading to a dramatic increase in the device temperature and power loss. This section aims to give a brief explanation of the physical process behind the temperature increase and its impact on solar cell performance.

### 1.5.1 Thermalization process

Photons absorbed by the solar cell provide energy to electrons to jump from the valance band into the conduction band, generating e-h pairs. It can happen that the photon energy is greater than the one needed by the electron to jump the band gap, *i.e.*,  $E > E_g$ . In this case, the electron jumps to a higher energy state.

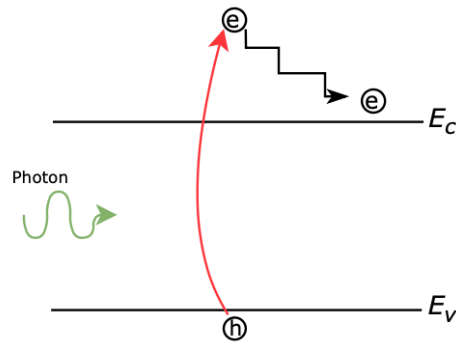


Figure 1.17: Thermalization loss mechanism

Then, it dissipates the excess energy as heat, relaxing to the lower available energy state of the conduction band (Figure 1.17). More precisely, the excess energy is transferred from the electron to lattice atoms through collisions. These events increase the lattice vibrations and, as a consequence, the thermal energy of the system, which leads to a rise of the solar cell temperature [15]. This process is unavoidable since the thermalization time is extremely short compared to the collection of excited carriers at the metal plates, about  $10^{-12}$  s [16].

Substantially, thermalization is the process that converts the excess electromagnetic energy given by a photon to an electron into heat, which turns to a rise of the  $pn$  junction temperature. It is the main intrinsic loss mechanism of solar cells based on crystalline semiconductors since a significant part of absorbed solar power is not converted into electricity.

### 1.5.2 Performance degradation

Since solar cells are semiconductor devices, they are sensitive to the increase of temperature. Normally, the PV module works at temperatures higher than the ambient one, it is influenced by the climate condition, solar radiation, and location. The typical operating temperature of a solar cell is 325 K or higher [17]. It is possible to compute this temperature through the following formula [18]:

$$T_{cell} = T_{air} + \left( \frac{NOCT - 293.15}{80} \right) S \quad (1.5.1)$$

where  $T_{air}$  is the ambient temperature, K, NOCT is the nominal operating cell temperature, K, and  $S$  is the solar irradiance,  $\frac{\text{mW}}{\text{cm}^2}$ . The NOCT for a c-Si solar cell has the value of 321 K [19]. Then, considering a solar irradiance of  $1 \frac{\text{kW}}{\text{m}^2}$  and an ambient temperature of 300 K, the silicon solar cell operating temperature is

335 K. In fact, the increase of temperature is even more significant in the PV systems because of the parasitic components.

The dependence of the solar cell performance from temperature arises from the temperature sensitivity of the band gap and the intrinsic loss mechanisms. Here, the temperature impact on some solar cells figures of merit is investigated.

### 1.5.2.1 Open-circuit voltage

The open-circuit voltage is strongly affected by the temperature variation. In particular, it reduces with the increase of temperature leading to a degradation of the solar cell performance (Left figure 1.18). The temperature sensitivity of the open-circuit voltage is described by the equation [20]:

$$\frac{dV_{OC}}{dT_c} = -\frac{\frac{E_{g0}}{q} - V_{CO} + \gamma \frac{kT_c}{q}}{T_c} \quad (1.5.2)$$

where  $E_{g0}$  is the band gap of the semiconductor linearly extrapolated to absolute zero, K,  $\gamma$  is a pure number that incorporates the temperature dependencies of several material parameters, which define the diode saturation current density, for example, in the case of silicon it is equal to 3. This equation shows the approximate linear relation between temperature and  $V_{OC}$ . Moreover, the two parameters are inversely proportional. Now, consider the equation of the open-circuit voltage (Eq. 1.4.30) and the one of the recombination current (Eq. 1.4.21). The temperature sensitivity is connected to the current recombination term, specifically, to the balance between generation and recombination of carriers and its variation with temperature. These mechanisms depend on different parameters, such as

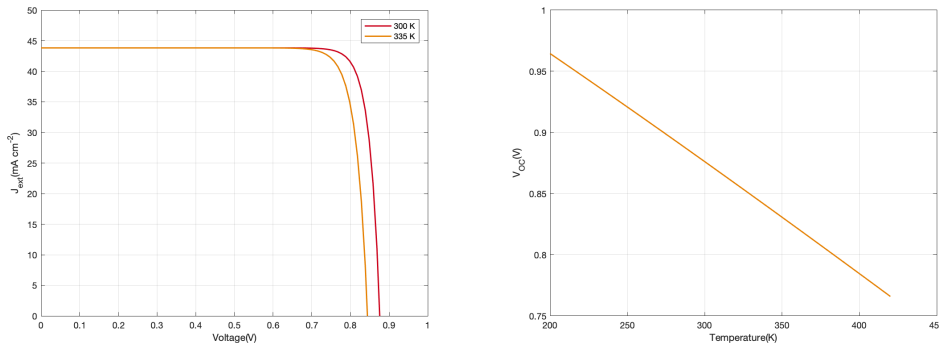


Figure 1.18: Left: JV characteristics of solar cells at different temperatures with respect to the voltage. Right: Open-circuit voltage with respect to temperature. ( $E_g = 1.12$  eV, terrestrial environment)

incident spectrum, reflection, concentrations of carriers, and type of recombination processes. However, the temperature sensitivity of the open-circuit voltage is mainly connected to the recombination processes, that is, on the concentrations of carriers. A more accurate analysis of this dependence is reported in the book “A Thermal Model for the Design of Photovoltaic Devices”[20].

Figure (1.18) displays the behavior of the open-circuit voltage with the increase of temperature. The solar cell working at standard operating temperature,  $T = 300$  K, has a higher voltage than the one at typical working conditions,  $T = 335$  K. The  $V_{OC}$  linearly decreases, as predicted by the equation (1.5.2), with a voltage-power coefficient equal to  $0.13 \frac{\%}{K}$ .

### 1.5.2.2 Short-circuit current

The temperature sensitivity of the short-circuit current is related to the energy gap temperature dependence, the incident solar spectrum and the variation of the collection efficiency with temperature (Eq. 1.4.19).

Then, to study the temperature dependence of this parameter, it is possible to analyze the variations of the silicon band gap variations with temperature described by the formula [21]:

$$E_g(T) = 1.17 - \frac{4.73 \cdot 10^{-4} T^2}{T + 636} \quad (1.5.3)$$

The impact of the energy gap variations on the  $J_{SC}$  can be evaluated using this equation in the computation of short-circuit current (Eq. 1.4.19). The band gap slightly decreases with the increase of temperature leading to an improvement

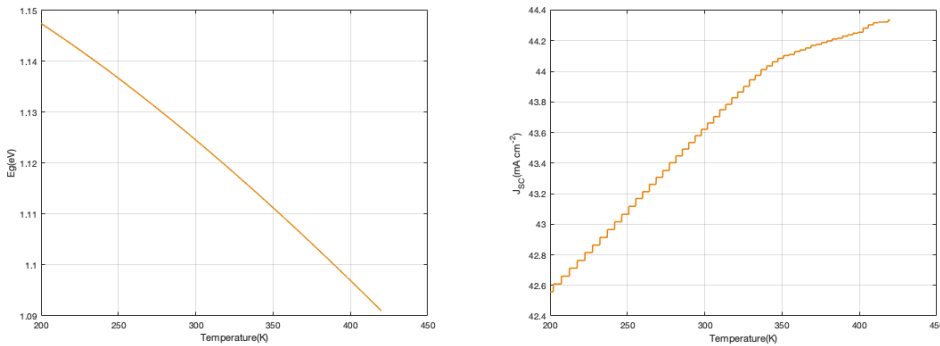


Figure 1.19: Left: The variation of the energy gap with respect to the temperature. Right: Short-circuit current with respect to temperature. (silicon solar cell, terrestrial environment)

of the  $J_{SC}$  (Figure 1.19). However, this current enhancement does not influence particularly the performance of the system compared to the open-circuit voltage [20]. The current-temperature coefficient is approximately  $0.02 \frac{\%}{K}$ , almost one order of magnitude lower than  $V_{CO}$ . The staircase behavior of the  $J_{SC}$  is due to the profile AM1.5g spectrum.

### 1.5.2.3 Efficiency

The decrease of the open-circuit voltage affects the electric power produced by the solar cell. Indeed, in left figure (1.20) is depicted the electric power of a silicon solar cell working in typical operating condition and in standard test condition. The maximum power point (MPP) of the cell at higher temperature is lower, which means that the photovoltaic conversion in this condition is reduced. The temperature dependence of the electric power, as the one of  $V_{CO}$ , is negative. The power-temperature coefficient is equal to  $-0.15 \frac{\%}{K}$  (Right figure 1.20).

The maximum efficiency is reached for materials with an energy gap of around  $1.35 \div 1.5$  eV (Left figure 1.21). In particular, the maximum conversion of solar power into electric power for a solar cell at 300 K is 33%, 1.8% more than the higher temperature case. Then, a large part of the power is converted into heat through thermalization. In right figure (1.21) is shown the variation of the efficiency with respect to the temperature for a silicon solar cell. It linearly decreases with an efficiency-temperature coefficient equal to  $0.051 \frac{\%}{K}$  (Right figure 1.21).

These are theoretical results useful to comprehend the temperature effect on the solar cell performance. Since the non-radiative recombination processes, band

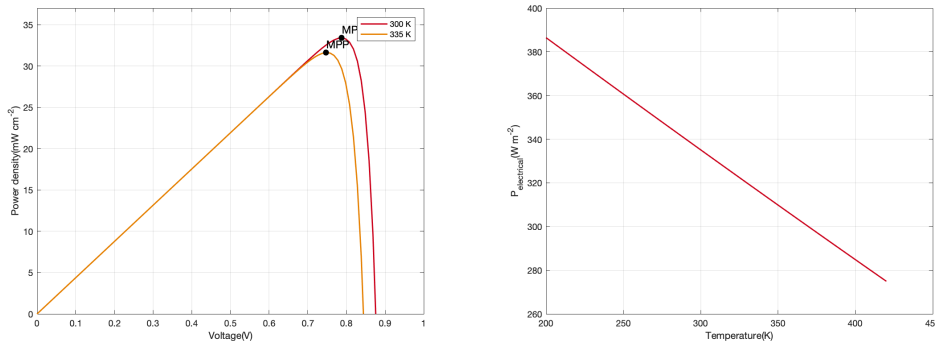


Figure 1.20: Left: Electric power with respect to the voltage for solar cells at different temperatures. Right: Maximum output power with respect to temperature. ( $E_g = 1.12$  eV, terrestrial environment)

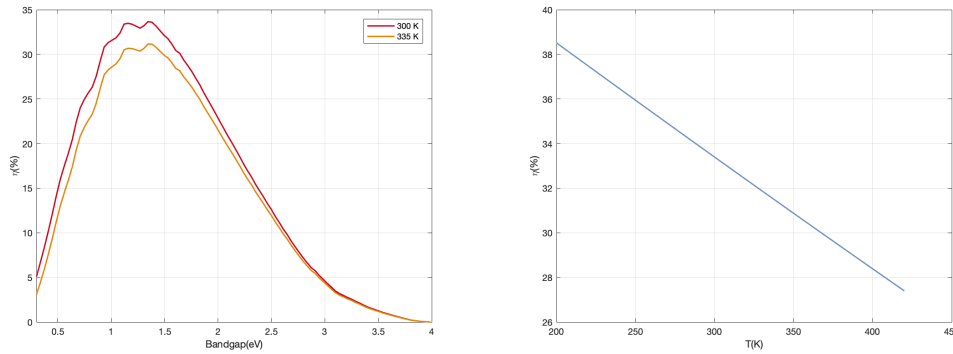


Figure 1.21: Left: The efficiency with respect the energy gap for solar cells with at different temperatures. Right: Efficiency with respect to temperature. ( $E_g = 1.12$  eV, terrestrial environment)

gap shifts, and real absorptivity of a solar cell are not considered, they might be an underestimation of the efficiency and power degradation. The recombination processes affects the performance producing a current and a voltage loss. First, it reduces the carriers that contributes to the electric current. Second, it decreases the concentration of carriers, and so the built-in voltage.

It has been experimentally observed that the increase of 1 K in a silicon solar cell leads to a decrease of the conversion efficiency of 0.082 %, and of the output power of 0.65% [22].

### 1.5.3 Lifespan degradation

The photovoltaic modules lifetime guaranteed by the manufactures is about 25 to 30 years, but the adverse weather and working conditions can reduce it. In particular, the operating temperature is one of the most impacting factors in the degradation phenomenon. High temperature can lead to defect in the modules, reducing their reliability. The aging rate of the solar cell array is strictly related to the working temperature of the solar cell, in particular for silicon PV module it doubles for every 10 K increase [23].

## 1.6 Cooling of solar cells

The reduction of solar cell operating temperature improves both the daily and the long-term generation of electric power. Hence, the overall amount of power produced by a solar cell is significantly improved. Furthermore, the same power

is generated by a lower number of photovoltaic panels, which means that less area has to be used for PV systems and can be addressed to other scopes. Considering the data reported in the right figure (1.1), an efficiency improvement of 1% is very significant. For example, it would entail an increase of 35 billion kilowatt-hours of the world production of electric power in 2030, which corresponds to a tenth of the electric power consumed in Italy in 2020. In this view, the cooling techniques of solar cells aim to develop a more efficient photovoltaic system. In recent years, a lot of different approaches for cooling PV panels have been developed. These techniques can require the employment of electric power or not. Then, they are classified in two main categories: active and passive. They are both based on non-radiative heat transfer mechanisms except for the passive radiative cooling technique.

### 1.6.1 Active

Active techniques exploit the movement of fluids by fan or pump to cool down the PV module. Forced airflow is the most common type of cooling. It is observed an efficiency increase up to 2%. The other cooling techniques are based on a coolant, such as water. The most effective methods are water spraying, forced water circulation, and liquid immersion. These techniques can reduce the operating temperature up to 40 K increasing the efficiency until 4% [24]. They are more effective than passive cooling techniques. However, active cooling can be expensive and not adaptable to large-scale implementation. Moreover, the increase of PV module output power has to be weighted by the extra power used by the cooling system.

### 1.6.2 Passive

The idea behind the passive cooling techniques is to improve the heat transfer characteristics of PV modules. It is carried out by including additional components, such as a heat sink. Since the need to find a scalable and effective solution for the temperature problem of solar cells, many passive cooling methods have been studied. The usual passive cooling strategies are based on non-radiative heat transfer through convection and conduction, such as phase-change material (PCM), heat pipe, heat exchanger, thermoelectric cooling. These techniques can theoretically reduce the temperature up to 15 K. They may increase the system cost and its complexity, limiting the widespread of these technologies. Recently, the passive radiative cooling technique has been introduced.

### 1.6.2.1 Radiative cooling technique

Raman et al. [25] in 2014 experimentally demonstrated that day-time radiative cooling is possible by using a photonic crystal. This material was designed to emit thermal radiation only in the atmospheric transparency window,  $8 \div 13 \mu\text{m}$ , and to reflect 97% of solar radiation, approximately  $0.3 \div 4 \mu\text{m}$ . It reaches a temperature below ambient even when exposed to sun radiation. The physical mechanism was deeply analyzed in Chapter 3. A first application of this technique to improve the solar cell efficiency was studied by Zhao et al. [26]. The idea is to substitute protecting glass layer of a solar cell with a photonic crystal that enhances the thermal radiation behavior of the system. They proposed different designs of radiative cooler compatible with the PV module, which theoretically reduces the temperature up to 17.6 K. Subsequently, a different photonic strategy was presented by Li et al. [27]. The radiative cooler is designed to enhance the transmission of the solar spectrum that contributes to photocurrent, about  $0.375 \div 1.1$ , and optimize the thermal emission. Moreover, in order to further reduce the temperature and preserve the solar cell, it reflects sub-band gap and UV radiation, which caused parasitic heat generation and degradation of the cell [28]. This approach enable to increase the solar cell efficiency of 1% [27].

This cooling technique has enormous potential. It is versatile since it can be applied for any type of solar cell and for concentrated and non-concentrated PV systems [29]. It can be employed alongside of other cooling techniques increasing the net cooling power of the system. The radiative cooler can be designed with multilayer structures made of cost-effective materials allowing a large-scale application. Another advantage of this technique is the self-cleaning functionality with particular structures of radiative coolers, such as silica pyramid structure [26].

# Chapter 2

## The fundamentals of thermal radiation

A deep understanding of the radiative cooling mechanism require the study of the nature of thermal radiation and its formulation. The explanation of this phenomenon is mainly related to two fields of physics, which are electromagnetism and quantum mechanics. The heat transfer by radiation is the most ordinary energy exchange that a human being experiences every day, for example, the heat that one perceives in the sun. The emission of thermal radiation is a property of matter, so every object on earth constantly releases radiation. The aim of this section is to provide the basic concepts and the mathematical formulation needed to understand the physical behavior of a thermal radiation.

### 2.1 The heat transfer mechanisms

First of all, heat is energy interchanged between different thermodynamic systems with mechanisms apart from thermodynamic work or transfer of matter. To be clearer, thermodynamic work is energy transferred with mechanisms that spontaneously exert macroscopic forces, e.g., pressure, gravity, electromagnetism, while the transfer of matter is the effective motion of mass, for example, chemical reactions, evaporation, separations of chemical compounds. The heat transfer is supported by two fundamental mechanisms:

- Thermal conduction and convection: the transfer of energy between objects by diffusion
- Thermal radiation: the transfer of energy between separated objects by the emission of electromagnetic waves

Actually, thermal convection is a special case of conduction. It is a macroscopic movement of molecules (fluid motion) outside of an imposed temperature gradient. The difference from the conduction case is that two bodies are not in contact but

they are separated by a fluid, which brings the energy from one body to the other. These heat transfer mechanisms can be clearly understood starting from their physical formulation. The law of heat conduction, also known as Fourier's law, is:

$$\mathbf{q} = -k\nabla T \quad (2.1.1)$$

where  $\mathbf{q}$  is a vector quantity and represents the local heat flux,  $\frac{\text{W}}{\text{m}^2}$ ,  $k$  is the conductivity of material,  $\frac{\text{W}}{\text{mK}}$ ,  $\nabla T$  is a vector quantity and represents the temperature gradient,  $\frac{\text{K}}{\text{m}}$ , which defines the direction of heat flow. Then, thermal conduction is ruled by the temperatures difference of the media involved in the heat transfer. For example, if the temperature is constant, *i.e.*, it is the same in all media of interest, the temperature gradient is equal to zero and so there is no heat propagation between them, the system is in *thermal equilibrium*<sup>1</sup>. This mechanism takes place through the random motion of particles of the bodies in contact, *i.e.*, there is a physical path for heat.

On the other hand, the phenomenon of heat transfer by thermal radiation is completely different. Initially, it is interesting to highlight two peculiar characteristics that heat radiation has. First, the thermal ray is in itself temperature independent, *i.e.*, the media temperature in which the radiation propagates does not affect it, for example, heat rays are focused on a body passing through a converging lens made of ice. After a while, the body starts to set a fire while the lens continues to be at constant temperature [30]. Second, the heat rays are independent of one another, for example, two radiation that crosses at a certain time remains as before the intersection takes place. However, the power radiated per unit surface from a black body<sup>2</sup> at temperature  $T$  is described by the Stefan-Boltzmann law:

$$E_B = \sigma T^4 \quad (2.1.2)$$

where  $E_B$  is the radiant flux of a black body,  $\frac{\text{W}}{\text{m}^2}$ ,  $\sigma$  is the Stefan-Boltzmann constant,  $\frac{\text{W}}{\text{m}^2\text{K}^4}$ . The radiated power depends on the fourth power of the temperature, hence, it is clear that every body, which temperature is different from 0 K, constantly emits and absorbs energy through thermal radiation, this is so-called Prevost's law. Hence, this mechanism is intrinsically related only to the temperature of the objects, *i.e.*, it occurs independently from what is present in

<sup>1</sup>It is one of conditions required for thermodynamic equilibrium. It occurs when the temperature of the two objects involved in the heat exchange is the same in any points of the space and at the same time.

<sup>2</sup>It is an idealized object that absorbs and emits radiation in every direction and wavelength. It will be better explained ahead in the chapter (Sec. 2.3).

the surroundings. In this case, the equilibrium between two objects in the same system that exchange heat by radiation is reached when the absorbed and emitted power of each of them is the same, *radiative equilibrium*.

The radiant flux (Eq. 2.1.2) has the same physical dimension of the local heat flux (Eq. 2.1.1), but it does not indicate the direction of heat rays since it defines the energy emitted by a black body.

It is important to notice another difference between these two heat transfer mechanisms: conduction requires a medium to transfer the heat, on the other hand, radiation does not require a supporting medium, since electromagnetic waves travel in vacuum.

## 2.2 Thermal radiation nature

In the previous section, the phenomenon of heat radiation was introduced and several properties of heat rays are discussed. Here, the focus is on the nature of heat radiation and the characterization of this object that carries energy from one point to the other.

To clarify the concept of heat radiation it is useful to consider the sun. At the same time, it emits light, which allows us to see, and heat that warms up our bodies. Hence, it is straightforward to imagine that they are the same thing, *i.e.*, *electromagnetic wave*. In particular, the visible range of the electromagnetic spectrum is a portion of the one of thermal radiation, which ranges from the shortest ultraviolet (UV) rays, dozens of nanometres, to the longest infrared (LRI), millions of micrometres. Therefore, the characterization of thermal radiation requires dealing with two branches of physics: electromagnetism and quantum physics. Then, it is possible to define some parameters in order to describe it: frequency, wavelength, wave number, energy, velocity.

Each electromagnetic wave has a certain energy and frequency, which are fixed by the source. These two parameters are strictly connected and described by the Planck relation, that is:

$$E = h\nu = \hbar\omega \tag{2.2.1}$$

where  $E$  is the energy, J,  $\nu$  is the frequency,  $\frac{1}{s}$ ,  $\hbar$  is the reduced Planck constant,

$\text{J} \cdot \text{s}$ ,  $\omega$  is angular frequency,  $\frac{\text{rad}}{\text{s}}$ , which equation are:

$$\begin{aligned}\hbar &= \frac{h}{2\pi} \\ w &= 2\pi\nu\end{aligned}\tag{2.2.2}$$

and  $h$  is the Planck constant:

$$h = 6.626070040 \cdot 10^{-34} \text{ J} \cdot \text{s}\tag{2.2.3}$$

Energy and frequency are absolute properties of the radiation, *i.e.*, they are independent of media in which they propagate. Instead, there are some parameters are affected by the presence of a medium, such as velocity. The speed of an electromagnetic wave is described by:

$$c = \frac{c_0}{n}\tag{2.2.4}$$

where  $c$  is the speed in a medium or *phase velocity*,  $\text{m}$ ,  $c_0$  is *the speed in free space*,  $\text{m}$ , that is:

$$c_0 = 299792458 \frac{\text{m}}{\text{s}}\tag{2.2.5}$$

and  $n$  is *refractive index* of the material in which the wave propagates. It is a pure number. This parameter is significant because it describes the electromagnetic behavior of the material. Actually, it quantifies the variation of speed radiation due to a medium. It is defined as:

$$n = \frac{c_0}{c} = \sqrt{\epsilon_r \mu_r}\tag{2.2.6}$$

where  $\epsilon_r$  and  $\mu_r$  are respectively the *relative* permittivity and permeability, which are pure number. While, electric permittivity,  $\frac{\text{F}}{\text{m}}$ , and magnetic permeability,  $\frac{\text{H}}{\text{m}}$ , are:

$$\begin{aligned}\epsilon &= \epsilon_0 \epsilon_r \\ \mu &= \mu_0 \mu_r\end{aligned}\tag{2.2.7}$$

where  $\epsilon_0$  is the permittivity of free space and  $\mu_0$  is the permeability of free space, their values are:

$$\begin{aligned}\epsilon_0 &= \frac{1}{c_0^2 \mu_0} = 8.854188 \cdot 10^{-12} \frac{\text{F}}{\text{m}} \\ \mu_0 &= 1.256637 \cdot 10^{-6} \frac{\text{H}}{\text{m}}\end{aligned}\tag{2.2.8}$$

In vacuum, the refractive index is equal to one, indeed,  $c = c_0$ .

Another parameter is the wavelength,  $m$ , that is:

$$\lambda = \frac{c}{\nu} \quad (2.2.9)$$

depending on velocity, it varies from one medium to the other. The frequency does not change, it is fixed by the source. The wavelength is an important parameter both for tradition<sup>3</sup> and because it is comparable with the space scales in our problems, *e.g.*, in nanostructures one can intuitively and qualitatively imagine which is the operation of the device by studying if its geometrical details are large or small compared to the wavelength. Substituting this expression in the Planck relation (Eq. 2.2.1), the relation between the energy and the wavelength of an electromagnetic wave is obtained:

$$E = h\nu = \frac{hc}{\lambda} \quad (2.2.10)$$

Eventually, the wave number,  $\frac{1}{m}$  is defined either:

$$k = \frac{1}{\lambda} \quad (2.2.11)$$

or through the *dispersion relation*:

$$k = w\sqrt{\epsilon\mu} \quad (2.2.12)$$

it represents the spatial frequency of the electromagnetic wave.

All of this theory is useful to understand the nature of heat radiation and will be the base for the development of electromagnetic model of radiative cooler in one of the last chapters.

## 2.3 Black body

The wave model can neither explain the radiative properties of gases nor the idea of the black body, so it is necessary to develop a quantum model.

One of the central concept in radiation heat transfer is that of a *black body*. It was introduced in 1860 by the physicist Gustave Kirchoff, then it has been rewritten

---

<sup>3</sup>In experimental physic, it was possible to make a direct measurement of this quantity, then, it was used to denote the color of a ray.[30]

in a more modern way, and its definition is:

*“A black body allows all incident radiation to pass into it (no reflected energy) and internally absorbs all the incident radiation (no energy transmitted through the body). This is true for radiation of all wavelengths and for all angles of incidence. Hence the black body is a perfect absorber for all incident radiation. [31]”*

This description explains the name provenance. All objects that absorb the visible light appear black to the eye, but their behavior for the other wavelengths can be different. Instead, the black body absorbs incident radiation at *any wavelengths*. It was adequately described by quantum mechanics and verified by experiments, using material such as black gold.

### 2.3.1 Quantitative definition

To better understand the concept of black body, it can be useful to provide a numerical definition of it based on optical quantities.

When a heat ray hits on an interface, *i.e.*, a surface between two different media, its power can be reflected, absorbed, and transmitted by it. These three optical phenomena are formulated as:

$$\begin{aligned}\rho &= \frac{\text{reflected power}}{\text{incident power}} \\ \tau &= \frac{\text{transmitted power}}{\text{incident power}} \\ \alpha &= \frac{\text{absorbed power}}{\text{incident power}}\end{aligned}\tag{2.3.1}$$

where  $\rho$  is the reflectivity,  $\tau$  is the transmissivity and  $\alpha$  is absorptivity. They are dimensionless quantities and represent the behavior of the object with respect to an electromagnetic field.

The situation can be summarized as the sum of these three terms:

$$\rho + \tau + \alpha = 1\tag{2.3.2}$$

To make a bit more quantitative description of these parameters, a plane wave incident on a planar interface between two media with different refractive indexes,  $n_1$  and  $n_2$ , is considered (Figure 2.1). We assume that the two layers are half-infinitely extended and their refractive index is real, *i.e.*, the material is not dissipative and

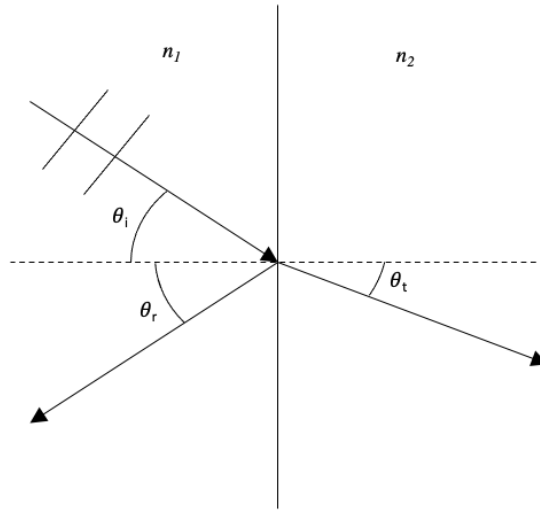


Figure 2.1: Plane wave incident on an interface

so the absorption term is eliminated from the equation (2.3.2). Then, according to the Fresnel equations [32] and considering the case of normal incidence,  $\theta_i=0^\circ$ , the reflection,  $r$ , and transmission,  $t$ , coefficients are:

$$r = \frac{n_1 - n_2}{n_1 + n_2} \quad t = 2 \frac{\sqrt{n_1 n_2}}{n_1 + n_2} \quad (2.3.3)$$

The reflectivity and the transmissivity are the square magnitude of this these two coefficient, that is:

$$\rho = |r|^2 \quad \tau = |t|^2 \quad (2.3.4)$$

these two coefficients quantify the power reflected and transmitted at the interface. To understand where the absorptivity term comes from we have to imagine a more complex structure, that is a dielectric slab (Figure 2.2). It is a stratified media composed of three layers, and each layer has a different refractive index:  $n_1$ ,  $n_2$  and  $n_3$ . The additional complication is required because, for example, if the first layer is assumed to be lossy, *i.e.*, dissipative layer, and half-infinitely extended, then, it is necessary to have infinite power at  $-\infty$  for a finite power at the interface. Based on this, the two external layers are assumed to be lossless, while the inner one is a lossy medium of finite length. Therefore, its refractive index is complex:

$$n_2 = n_2 - i\kappa_2 \quad (2.3.5)$$

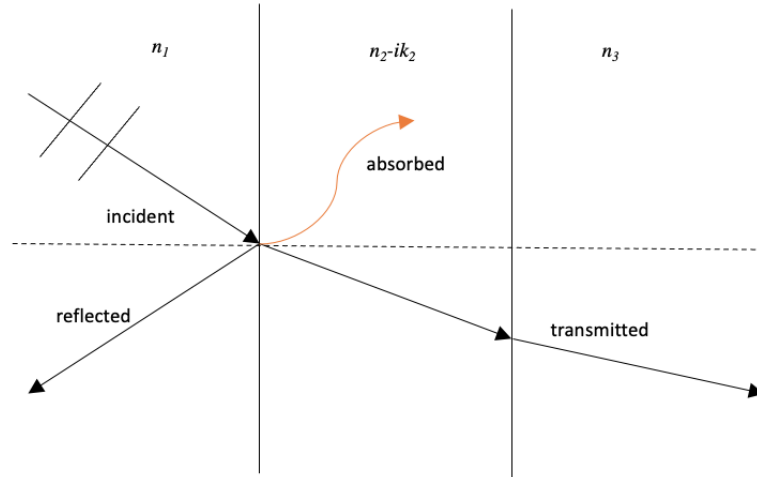


Figure 2.2: Plane wave incident on dielectric slab

where  $\kappa$  is the *extinction or absorption coefficient*<sup>4</sup>, and defines the quantity of attenuation of electromagnetic wave that propagates through the material,  $n_2$  indicates the phase velocity of the wave. After the computation of the reflectivity and transmissivity, it is possible to evaluate the absorptivity from the equation (2.3.2) as:

$$\alpha = 1 - \rho - \tau \quad (2.3.6)$$

The reflectivity and transmissivity can be calculated by different methods, such as Transmission line technique, Transfer matrix method.

Finally, the black body properties can be represented in numerical form as:

$$\begin{cases} \rho = 0 \\ \tau = 0 \\ \alpha = 1 \end{cases} \quad (2.3.7)$$

Since, all the power of incident radiation is absorbed by the black body, the reflectivity and transmissivity are equal to zero.

So far, to make simpler and clearer the explanation, the direction and spectral dependencies of these parameters are not considered. First, the dependence from the incidence angle,  $\theta_i$ , strongly affects the response of the medium to the electromagnetic wave, as it will be shown in the last chapter. Yet, this is more

<sup>4</sup>Notice that  $\kappa$  are positive in passive medium because of the phasor time convention  $\exp(i\omega t)$ . With the time convention adopted, a negative  $\kappa$  characterize active media, such as laser media.[33]

complicated in the 3D case, where there is also the azimuth angle,  $\varphi$ , to take into account. Second, the dielectric properties of a medium depend on the wavelength. For example, considering again the dielectric slab, where the thickness of the central layer is identified with  $l_{AB}$ , it is possible to highlight three limit cases:

- $\lambda$  is much bigger than  $l_{AB}$ : the central layer is almost invisible from the wave perspective
- $\lambda$  is comparable to  $l_{AB}$ : the slab behaves in the usual way, that is, the incident power is partially reflected, partially transmitted and partially absorbed in relation to the incident angle and refractive indexes
- $\lambda$  is much smaller than  $l_{AB}$ : the central layer absorbs all the incident power and so the third layer is negligible

Here it can be noted that controlling the thickness of the layer changes its response to an electromagnetic wave. Hence, it is a first example of the possibility of engineering the optical properties of a material.

Another example of wavelength dependence is the dispersion phenomenon, *i.e.*, electromagnetic waves of different wavelengths travel in a medium at different speeds. This mechanism is described by refractive index dependence on wavelength (and frequency),  $n(\lambda)$ . Eventually, the three terms of equation (2.3.2) can be rewritten highlighting their dependencies, that is:

$$\rho(\lambda, \theta, \varphi) \quad \tau(\lambda, \theta, \varphi) \quad \alpha(\lambda, \theta, \varphi) \quad (2.3.8)$$

In this view, it is clear that an object could behave more or less as a black body only in a certain range of wavelength. As said in other words: an ideal black body absorbs all the radiation independently of  $\lambda$ ,  $\theta$ ,  $\varphi$ . So, it is straightforward to use the conceptual definition of it as a benchmark against which real structures are compared. Indeed, it will be used to define some parameters that describe the radiative behavior of a material.

Now that the properties of black body are deeply analyzed, some ideal experiments will be studied to further clarify its behavior.

### 2.3.2 Black body as perfect emitter

The Prevost's law ensures that a black body emits radiation when its temperature is different from the absolute zero.

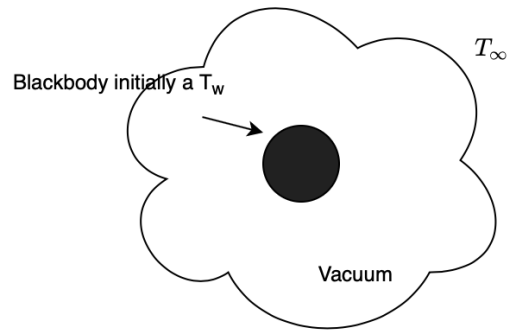


Figure 2.3: Black body in evacuated chamber at constant temperature

Consider the scenario represented in figure (2.3). There is a black body at the initial temperature,  $T_w$ , in an evacuated chamber, *i.e.*, no medium is present between the wall and the black body. Since it is smaller than the cavity no conduction and convection can take place, the only heat transfer mechanism that occurs is the radiation one. It is assumed that the walls temperature of the cavity is fixed and cannot change,  $T_\infty$ , and the black body initial temperature is higher. Before the beginning of the experiment, it is essential to observe that in these conditions the radiative and thermal equilibrium represent the same state of the system, *i.e.*, when the radiation fluxes are the same, the temperatures of the two objects are also the same.

Initially, the black body has to release energy in the form of heat radiation to reach equilibrium. Consequentially, it reduces its own temperature, and after a while, the equilibrium is reached, that is, the net exchange of energy with the surroundings is zero. It is a dynamic equilibrium: the black body emits the same radiation that it absorbs from the surrounding environment. In this view, assuming that the cavity has the same emission properties as the black body then the equilibrium temperature is  $T_\infty$ .

Since the absorptivity and emissivity spectra of a black surface coincide, it is the best possible emitter and absorber at any temperature. This concept will be deeper analyzed in the section dedicated to the absorptivity parameter (Sec. 2.5.2).

### 2.3.3 Isotropic emitter

In the previous experiment, the position and orientation of the black body inside the cavity were not mentioned because its radiation field is independent from these

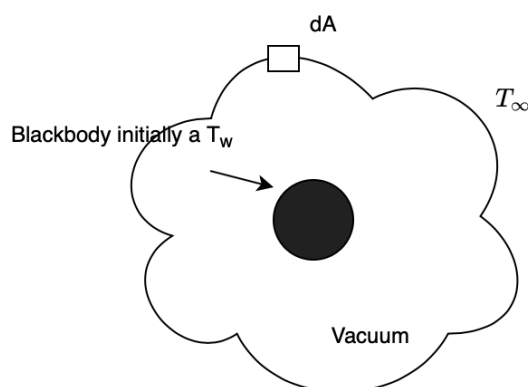


Figure 2.4: Black body in evacuated chamber radiatively inactive apart from  $dA$

parameters. For example, considering the previous scenario, if the black body is moved from the center of the chamber closer to the wall nothing changes from the radiative point of view. Since it keeps absorbing and emitting the same amount of radiation, the radiative-thermal equilibrium is maintained. The same happens if the black body is rotated in any direction. Then, the position does not influence the emissivity. Furthermore, these statements are true for any type of black body shape.

Now, consider the scenario represented in figure (2.4). This time only a small area,  $dA$ , of the enclosure is radiatively active. Since the wall is isothermal, a portion of it constantly releases the same quantity of energy. To reach the radiative equilibrium, the black body emits in the direction of the small area the same amount of radiation that it absorbs from  $dA$ . In doing this, it emits and reabsorbs its radiation in the other directions. In this way, all incoming and outgoing fluxes are balanced. The intensity of black body radiation is imposed by the small area temperature. In other words, it has the maximum<sup>5</sup> emission in all the directions to balance the maximum absorption coming from the small area direction. This experiment shows that the radiation emitted by a black body has a uniform intensity in all the direction of propagation since moving the small area along the wall the equilibrium is maintained. Then, the black body is an isotropic emitter. Obviously, the same is true for the radiation absorbed by it, *i.e.*, the absorptivity is independent from the angles of incidence.

<sup>5</sup>it is used the adjective “maximum” because the black body is the best emitter and absorber ideally obtainable.

### 2.3.4 Uniform spectral emitter

Using a similar idea, it is possible to study the emissivity of a black body for different wavelengths. If a cavity designed to emit only in a certain range of wavelengths from  $\lambda$  to  $\lambda+d\lambda$  is considered, the heat exchange takes place in all directions but only for specific wavelengths. Hence, the black body emits at any wavelength but absorbs only in the defined interval imposed by the enclosure property, so the interval is reached when the radiation of black body are equivalent to the one of the enclosure for each wavelength of the interval. Changing  $d\lambda$ , the system remains in equilibrium, it follows that the black body radiation has a uniform intensity for every wavelength. Actually, the black body reaches the equilibrium reabsorbing the radiation that are reflected by the enclosure.

### 2.3.5 Effect of temperature on radiation

In all the situations that have been analyzed up to now, the final result is always the same, that is, after a while the black body passes from an initial temperature,  $T_w$  to the temperature of enclosure,  $T_\infty$ . This happens independently of the shape or size of the black body and/or the cavity. Hence, the only parameter that affects the heat radiation of a black body in vacuum is the *temperature*. Also, it is possible to state that radiation strength is *directly proportional* to the temperature. To convince of this fact, one can think about the second law of thermodynamics, which states that energy cannot go from a cold body to a hot body without external work applied to the system. Then, the energy radiated by a body,  $E$ , must be proportional to the temperature:

$$E \propto T \tag{2.3.9}$$

It is also defined by Stefan-Boltzmann's law (Eq. 2.1.2).

## 2.4 Planck's law

In the previous sections, the various radiative properties of the black body were analyzed. Here, the focus is on the definition and formulation of the intensity of its radiation,  $I_{\lambda b}$ , providing a more quantitative description of its behaviour. To understand radiative heat transfer, the most significant points of the entire process to obtain Planck's law are reported here.

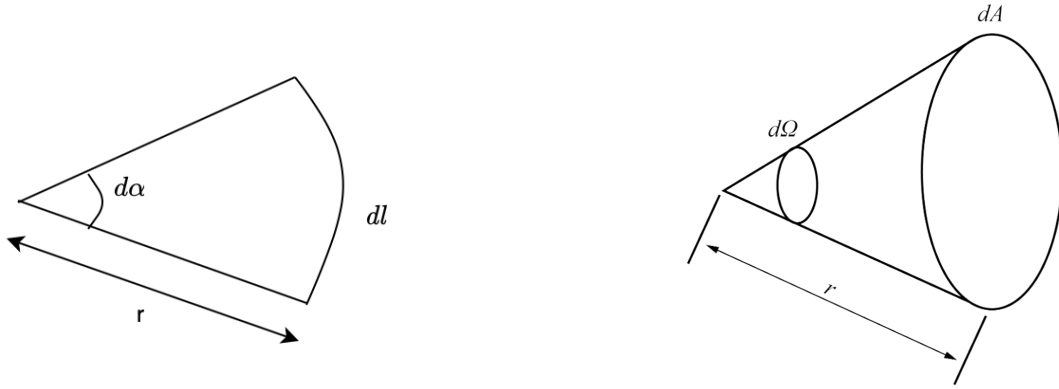


Figure 2.5: Left: Planar angle. Right: Solid angle.

### 2.4.1 Solid angle

An important geometrical concept is the one of solid angle. It is better to start from the definition of planar angle: imagine to have a segment of circle of infinitesimal length,  $dl$ , and radius,  $r$ . Then, the corresponding infinitesimal angle,  $d\alpha$ , is:

$$d\alpha = \frac{dl}{r} \quad (2.4.1)$$

it is measured in radians, rad, which is a pure number.

Now, this concept is extended to the three dimensions space, that is, the solid geometry. The arc length is substituted by the infinitesimal area of a sphere,  $dA$ , with radius,  $r$  (Figure 2.6). The infinitesimal solid angle is defined as:

$$d\Omega = \frac{dA}{r^2} \quad (2.4.2)$$

its measurement unit is steradians, sr.

It represents the amplitude of the angle subtending the portion of spherical surface that is compared to the square of the sphere radius.

### 2.4.2 Set up the heat transfer problem

Considering the scenario in figure (2.4). To evaluate the power absorbed by the small area, conceptually, it is necessary to multiply the total power emitted by the black body by a quantity that represents the portion that intercepts the radiation. This quantity is the solid angle. Indeed, its definition implies the presence of two actors: an infinitesimal area, to which the solid angle refers, and the area subtended by it. It fits perfectly the radiative heat transfer mechanism between two objects: a giver, *i.e.*, a surface that emits radiation, and a taker, *i.e.*, a surface

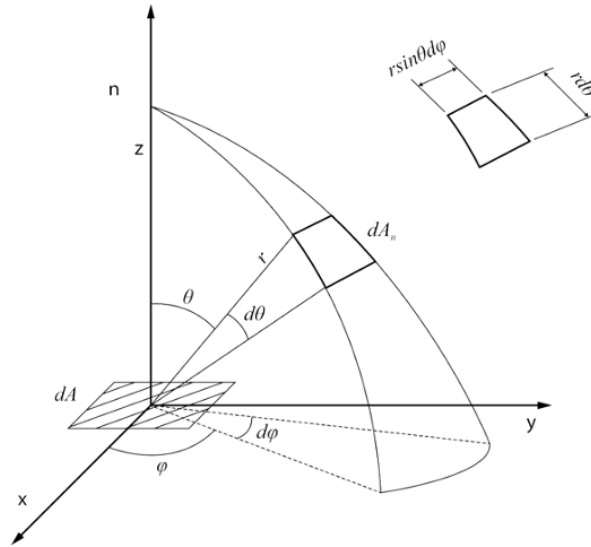


Figure 2.6: Exchange of heat radiation between two infinitesimal areas

on which some radiation strikes.

To represent the scenario, it is fundamental to employ the *spherical coordinate system*. Two infinitesimal areas are defined: the emitting area,  $dA$  and the interception area,  $dA_n$  (Figure 2.6). The position of  $dA_n$  with respect to  $dA$  is defined by the *polar angle*,  $\theta$  and the *azimuthal angle*,  $\phi$ . The first one is between the zenith,  $z$ , and the plane  $(x,y)$ . The latter is defined between the  $x$  and  $y$  coordinates. The solid angle refers to  $dA$ . The interception area is defined as the spherical element area at a distance  $r$  from the emitting area. It is generated by varying infinitesimally the two angles,  $d\phi$  and  $d\theta$ , so its equation is:

$$dA_n = r \sin \theta d\phi r d\theta \quad (2.4.3)$$

Recalling the equation (2.4.2) and substituting in it the infinitesimal area expression, it is possible to provide an operative expression of the solid angle, that is:

$$d\Omega = \frac{dA}{r^2} = \frac{r^2 \sin \theta d\phi d\theta}{r^2} = \sin \theta d\phi d\theta \quad (2.4.4)$$

As already mentioned, the aim of this chapter is to study the heat transfer by thermal radiation between surfaces of finite area. Then, it is interesting to do a preliminary exercise in order to become more familiar with the concept of solid angle. Consider a surface that isotropically emits<sup>6</sup> radiation only in a hemisphere.

<sup>6</sup>Actually, the surface does not emit any heat rays, they are generated in the interior of the object and they pass through the surface. So, this expression is used for sake of brevity [30].

In this view, the solid angle has to be calculated for such a hemisphere. So, it is necessary to integrate along the two angles, as follow:

$$\Omega = \iint d\Omega = \int_0^{2\pi} \int_0^{\frac{\pi}{2}} \sin\theta \, d\varphi \, d\theta = 2\pi [-\cos\theta]_0^{\frac{\pi}{2}} = 2\pi \text{ sr} \quad (2.4.5)$$

The concept of solid angle is essential from the study of radiative heat exchange between objects in the same environment. They can be modelled as finite surfaces with a certain position and direction that usually irradiates heat in different directions.

### 2.4.3 Projected area

Before the introduction of Plank's law It is useful to present another important concept, which is the projected area. The orientation of the emitting surface with respect to the intercepting surface affects the radiative heat transfer. Indeed, if the surfaces are perfectly facing each other, then the power transferred will be maximum, but if instead they are not parallel, then it will be lower. This is true in the case of non-uniform directional radiation, obviously, for the black body case there is no difference. Therefore, it is crucial to take the orientation of emitting surface into account through the formula of projected area, which is:

$$dA_p = dA \cos\theta \quad (2.4.6)$$

where  $\theta$  is polar angle, *i.e.*, it is defined between the normal of the absorbing area and the emitting area. In figure (2.7), it is depicted the emission case of the area  $dA$ , in the absorbing on the image is reversed.

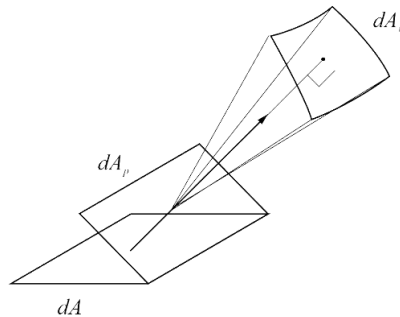


Figure 2.7: Projected area  $dA_p$

### 2.4.4 Spectral radiation intensity

It is well known that a surface can emit radiation in any directions and for any wavelengths. Furthermore, the radiated power incident on a surface can come from a reflection, a transmission or a emission. Hence, the definition of a quantity which takes into account these properties and allows to evaluate the heat flux for precise interval of these parameters is mandatory. Then, it is possible to define the *spectral radiation intensity* or *spectral radiance*,  $I_{\lambda,e}$ <sup>7</sup>, as [34]:

$$I_e(\lambda, T, \theta, \varphi) = \frac{\partial Q}{\partial A \partial \Omega \partial \lambda} \quad (2.4.7)$$

The unit of measurement is  $\frac{\text{W}}{\text{sr m}^2 \mu\text{m}}$ .

$I_{\lambda,e}$  is the power, W, emitted by a surface in the direction  $\theta$  and  $\varphi$ , per unit wavelength interval around  $\lambda$ ,  $\mu\text{m}$ , per unit of area,  $\text{m}^2$ , per unit of solid angle, sr. It is important to notice that the temperature dependence of the radiance is embedded in the energy rate term,  $dQ$ . Integrating the spectral intensity along the angles and the wavelength, the radiative heat flux is obtained, so it can be related with the heat flux calculated in conduction and convection cases (Eq. 2.1.1). Then, it is possible to apply the heat flux balance equation to find the equilibrium temperature of the surface under test, as will be shown in the next chapters.

The spectral radiation intensity and the preliminary consideration on solid angle generate a convenient platform to set up a quantitative theory of black body radiation. Therefore, the idea was to relate  $I_{\lambda,e}$  to black body concept exploiting the its properties, which is the simplest case since the intensity of radiation is dependent only on temperature, to find a preliminary expression of the radiance.

### 2.4.5 Black body hemispherical emissive power

Taking into consideration the emissivity angular profile of the black body, it is possible to define the power emitted per unit area by a black surface, which is the *hemispherical spectral emissive power*, as:

$$E_b(\lambda, T) = \int_0^{2\pi} \int_0^{\frac{\pi}{2}} I_b(\lambda, T) \cos\theta \sin\theta \, d\theta \, d\varphi = \pi I_b(\lambda, T) \quad (2.4.8)$$

the unit of measurement is  $\frac{\text{W}}{\text{m}^2 \mu\text{m}}$ .

Integrating along the two angles the angular dependence is eliminated, but the

---

<sup>7</sup>The “ $\lambda$ ” indicates that this is a spectral quantity. The “e” indicates that emitted radiation is considered.

spectral one remains. Then, evaluating this quantity for an interval of wavelengths, the *total hemispherical emissive power*, which corresponds to the radiative flux of the surface, is obtained:

$$E_b(T) = \int_0^\infty E_b(\lambda, T) d\lambda \quad (2.4.9)$$

Substituting  $E_{\lambda, b}$  whit (the (2.4.8):

$$E_b(T) = \int_0^\infty \int_0^{2\pi} \int_0^{\frac{\pi}{2}} I_b(\lambda, T) \cos\theta \sin\theta \, d\theta \, d\varphi \, d\lambda = \pi I_b(T) \quad (2.4.10)$$

the unit of measurement is  $\frac{\text{W}}{\text{m}^2}$ .

The black body hemispherical emissive power is proportional to its radiation intensity by a factor  $\pi$ . This equation is used to relate hemispherical quantities.

## 2.4.6 Planck's law

The first expression of spectral radiation intensity of blackbody was the Rayleigh-Jeans's law, that is:

$$I_b(\nu, T) = \frac{2\nu^2}{c^2} k_B T \quad (2.4.11)$$

Its unit is  $\frac{\text{W}}{\text{sr m}^2 \text{Hz}}$ .

where  $k_B$  is the Boltzmann constant:

$$k_B = 1.38064910^{-23} \frac{\text{J}}{\text{K}} \quad (2.4.12)$$

but it worked only for low frequencies. The problem is that in the Rayleigh-James version does not takes into account the quantum nature of light, namely, the photoelectric effect. So, the integral of distribution goes to infinity for high energies, that is, the *ultraviolet catastrophe*. Hence, Planck adopted a statistical mechanics approach, *i.e.*, a probabilistic approach, and proposed the well known Planck's law:

$$I_b(\nu, T) = \frac{2h\nu^3}{c^2} \frac{1}{e^{\frac{h\nu}{k_B T}} - 1} \quad (2.4.13)$$

Its unit is  $\frac{\text{W}}{\text{sr m}^2 \text{Hz}}$ .

The Planck's law expressed in term of energy is obtained substituting the Planck

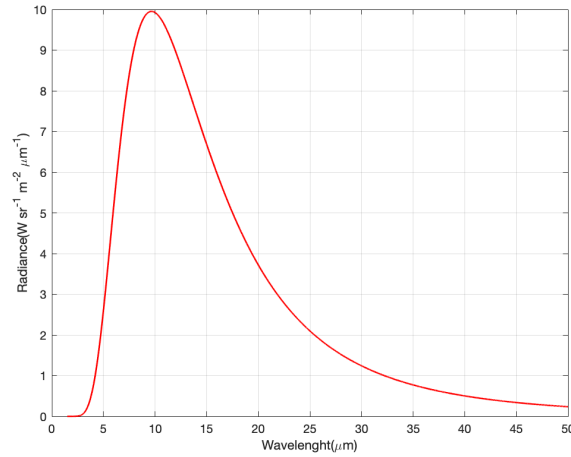


Figure 2.8: Planck's Law for temperature of 300 K

relation (Eq. 2.2.1) in the previous equation, then:

$$I_b(E, T) = \frac{2E^3}{h^2 c^2} \frac{1}{e^{\frac{E}{k_B T}} - 1} \quad (2.4.14)$$

Its unit is  $\frac{\text{W}}{\text{sr m}^2 \text{J}}$ .

For completeness, the Planck's law with respect to the wavelength is computed. An infinitesimal increment of wavelength does not correspond directly to an infinitesimal change of frequency, which instead is directly proportional to E, because it is known that:

$$\nu = \frac{c}{\lambda} \quad (2.4.15)$$

Then:

$$d\nu = -\frac{c}{\lambda^2} d\lambda \quad (2.4.16)$$

So, converting the  $I_{\lambda,e}$  to  $I_{\nu,e}$  needs:

$$|I_{\lambda,e} d\lambda| = |I_{\nu,e} d\nu| \quad (2.4.17)$$

Finally, the equation (2.6) is expressed as:

$$I_b(\lambda, T) = \frac{2hc^2}{\lambda^5} \frac{1}{e^{\frac{hc}{\lambda k_B T}} - 1} \quad (2.4.18)$$

Its unit is  $\frac{\text{W}}{\text{sr m}^2 \text{m}}$ .

This expression describes the *spectral* power emitted by a black body per unit of projected area, per unit solid angle. It was experimentally verified and depends on

the black body absolute temperature and wavelength. In figure (2.8), it is possible to see the graphical representation of this law for a black body at the ambient temperature. Notice that, a body at ambient temperature has the majority of the spectrum in the mid-infrared region.

The Planck’s law be the basis of all discussions on radiative heat transfer through the thesis and it is used in order to define some very important parameters of materials, such as emissivity.

## 2.5 Non-black body surface

So far, the most relevant formulas defined are valid for an ideal black body. Actually, real bodies emit only for some ranges of wavelength and the intensity is non-uniform in all the directions. Hence, there are two non-idealities: the spectral one and the directional one (Figure 2.9). Furthermore, their radiative properties even changes due to external factors, such as, temperature. In this section various parameters are introduced to characterize the radiative behavior of real bodies in order to their spectral radiation intensity can be evaluated. These parameters will be defined using the black body as a benchmark against which to compare real bodies. Most of the material presented in this section is strongly based on two books “Essentials of Radiation Heat Transfer” [34] and “Thermal Radiation Heat Transfer” [31].

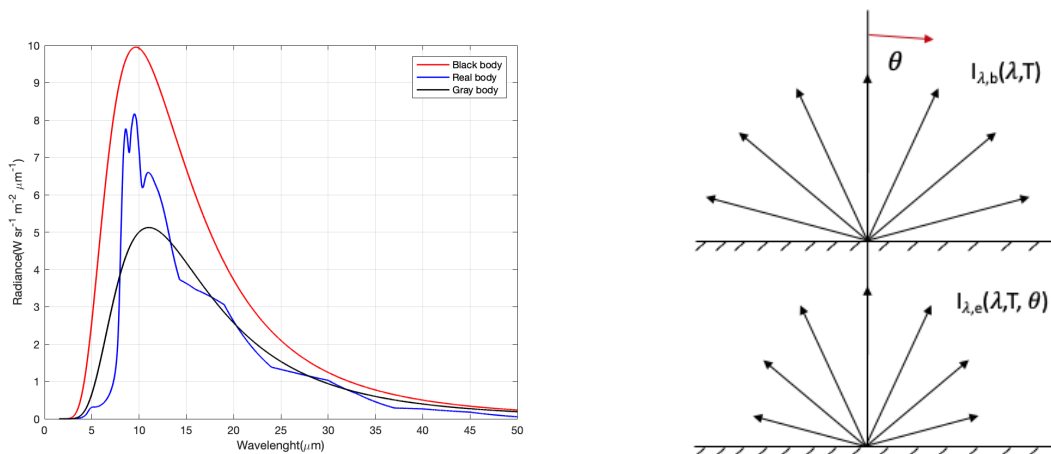


Figure 2.9: Left: the spectral non-ideality (bodies temperature of 300 K). Right: the directional non-ideality

## 2.5.1 Emissivity

The first parameter introduced is the emissivity, which describes the emission profile of a object. In other words, it specifies the quantity of power radiated by it for each wavelength and direction. First, it is presented the concepts of a gray and diffuse surface to study the emissivity without the directional and spectral dependencies. Later, the definition of the real body emissivity is introduced,  $\epsilon(\lambda, \theta, \varphi)$ .

### 2.5.1.1 Gray and diffuse surface

Usually, the curves of spectral radiation intensity of a real body have very complex profiles with respect to the one of a black body at the same temperature (Figure 2.9), they vary with the wavelength and direction. Then, the idea is to eliminate these dependencies approximating these curves with the one of a black body.

First, the focus is on spectral dependence. It is removed substituting the function that represents the wavelength radiance variation with the one of the black body at a certain temperature, *gray body* (Left figure 2.9). The gray body temperature,  $T_g$ , is computed by imposing the equality of the two areas subtend by the real and black surface curves and varying the temperature of the latter. Since the area must be equal,  $T_g$  will be lower than the real surface temperature. For example, in left figure (2.9), it is represented the radiance of a real surface and a black body at 300 K, respectively the blue and red line. Instead, the black line depicts the gray body approximation of the blue line, it corresponds to the radiance of a black body at 262.6745 K.

The ratio of the gray body radiance and the black body radiance is independent from the wavelength, and it can be written as:

$$\frac{I_g(\lambda, T_g)}{I_b(\lambda, T)} = f(\lambda) \quad (2.5.1)$$

where  $T$  is the temperature of the black body, which is different from  $T_g$ . This ratio is called *emissivity* and is dimensionless. In particular, it is the emissivity of a gray body in this case. Since the two radiance has the same profile the ratio is constant and smaller than one for any wavelength. I means that the gray body partially absorbs the incident power.

Now, the directional dependencies of the real body radiance are studied. The intensity of radiation emitted by a real surface might change for different polar angles,  $\theta$ , or even for azimuthal angles,  $\phi$ , in 3D case (Figure 2.9). Using the same

idea of the gray body, it is possible to get rid of the directional dependencies, *diffuse surface*. Its emissivity is defined as:

$$\frac{I_d(\lambda, T_d, \theta, \varphi)}{I_b(\lambda, T)} \neq f(\theta, \varphi) \quad (2.5.2)$$

it is constant in any direction.

If it is possible to assume that our real body is simultaneously gray and diffuse, then the emissivity does depend only on temperature: this is the *gray-diffuse approximation*. Different real surfaces at the same temperature have different emissivity profiles, then, they are approximated with gray body of different temperatures.

These approximations can be useful for doing some rough calculations and reducing the computational load, for example, it simplifies the evaluation of the power density radiated by a real surface usually introducing a small error.

### 2.5.1.2 Spectral directional emissivity

The real bodies emitted power depends on wavelength, position, orientation and directions, comparing it with the one emitted by the black body, which is uniform for every variables, a parameter that characterizes the emission of a real boy is obtained, *i.e.*, the *spectral directional emissivity*. Hence, it is defined as:

$$\epsilon'(\lambda, T, \theta, \varphi) = \frac{I_e(\lambda, T, \theta, \varphi)}{I_b(\lambda, T)} \quad (2.5.3)$$

where  $\epsilon'_\lambda(\lambda, T, \theta, \varphi)$  is a dimensionless function that varies from 0 to 1, except in the case of a black body in which it is one for all wavelengths and directions. Both numerator and denominator are calculated for the same temperature. Rewriting the equation, it is possible to find an expression for the evaluation of the radiance of a real body, that is:

$$I_e(\lambda, T, \theta, \varphi) = \epsilon'_e(\lambda, T, \theta, \varphi) I_b(\lambda, T) \quad (2.5.4)$$

this formula is extremely important, accepting that the spectral emissivity was characterized in some way, so (2.5.4) becomes an operative formula to assess the spectral radiation intensity emitted from a real surface of interest.

The spectral directional emissivity is the representation of the real body from a radiative point of view.

In order to become more familiar with these formulas and understand better the

previous concepts, the emissivity for gray body and diffusive body are reported. The first is independent from the wavelength, so:

$$\epsilon'(\lambda, T, \theta, \varphi) \rightarrow \epsilon'_g(T, \theta, \varphi) \quad (2.5.5)$$

The latter is independent from the two angles, so:

$$\epsilon'(\lambda, T, \theta, \varphi) \rightarrow \epsilon'_d(\lambda, T) \quad (2.5.6)$$

the diffusive body approximation can even be applied for only one of the two angles. When these approximations can be employed, they significantly simplify the calculation.

### 2.5.1.3 Spectral hemispherical emissivity

Usually, the average emissivity values has to be employed due to the lacking of data for all spectral ranges and directions, or for reducing the computational load. Therefore, it is important to calculate the directional average of emissivity, *i.e.*, the *spectral hemispherical emissivity*, which mathematical definition is:

$$\epsilon(\lambda, T) = \frac{E(\lambda, T)}{E_b(\lambda, T)} \quad (2.5.7)$$

The spectral hemispherical power,  $E_\lambda(\lambda, T)$ , is obtained by integrating the spectral radiation intensity per unit of solid angle. Then, recalling (2.4.8):

$$E(\lambda, T) = \int_0^{2\pi} \int_0^{\frac{\pi}{2}} I_e(\lambda, T, \theta, \varphi) \cos\theta \sin\theta \, d\varphi \, d\theta \quad (2.5.8)$$

using (2.5.4), the previous expression becomes:

$$E(\lambda, T) = \int_0^{2\pi} \int_0^{\frac{\pi}{2}} \epsilon'(\lambda, T, \theta, \varphi) I_b(\lambda, T) \cos\theta \sin\theta \, d\varphi \, d\theta \quad (2.5.9)$$

substituting the equation (2.5.9), (2.4.10) in (2.5.7) and simplifying, the expression of spectral hemispherical emissivity is obtained:

$$\epsilon(\lambda, T) = \frac{1}{\pi} \int_0^{2\pi} \int_0^{\frac{\pi}{2}} \epsilon'(\lambda, T, \theta, \varphi) \cos\theta \sin\theta \, d\varphi \, d\theta \quad (2.5.10)$$

#### 2.5.1.4 Directional total emissivity

Here, the spectral directional emissivity is integrated along the wavelength not the angles. So, it is called *directional total emissivity* because it accounts for all the spectral components. It is defined as:

$$\epsilon'(T, \theta, \varphi) = \frac{I'_e(T, \theta, \varphi)}{I'_b(T)} \quad (2.5.11)$$

The numerator is calculated integrating the spectral radiation intensity and obtaining the *directional total intensity*:

$$I'_e(T, \theta, \varphi) = \int_0^\infty I_e(\lambda, T, \theta, \varphi) d\lambda \quad (2.5.12)$$

Then, the denominator is evaluated in the same way obtaining the *black body total intensity*:

$$I'_b(T) = \int_0^\infty I_b(\lambda, T) d\lambda = \frac{\sigma T^4}{\pi} \quad (2.5.13)$$

Here, the Stefan-Boltzmann law appears (Eq. 2.1.2) and it is divided by the  $\pi$ , which comes from (2.4.10).  $\sigma$  is the fundamental Stefan-Boltzmann constant:

$$\sigma = \frac{\pi^2 k^4}{60 \hbar^3 c^2} = 5.67 \cdot 10^{-8} \frac{\text{W}}{\text{m}^2 \text{K}^4} \quad (2.5.14)$$

Finally, substituting (2.5.12) and (2.5.13) in (2.5.11):

$$\epsilon'(T, \theta, \varphi) = \frac{\int_0^\infty I_b(\lambda, T) \epsilon'(\lambda, T, \theta, \varphi) d\lambda}{\frac{\sigma T^4}{\pi}} \quad (2.5.15)$$

it is a dimensionless number.

#### 2.5.1.5 Hemispherical total emissivity

It is important to introduce this emissivity because it leads to the concepts of total emissive power of a body. Then, the radiance is integrated with respect the three variables: wavelength, polar angle and azimuthal angle, such as in equation (2.4.10):

$$E_b(T) = \int_0^\infty \int_0^{2\pi} \int_0^{\frac{\pi}{2}} I_b(\lambda, T) \epsilon'(\lambda, T, \theta, \varphi) \cos\theta \sin\theta d\theta d\phi d\lambda \quad (2.5.16)$$

Its unit is  $\frac{W}{m^2}$ .

Recalling the emissive power of a black body, the hemispherical total emissivity is defined as:

$$\epsilon(T) = \frac{E_e(T)}{E_b(T)} \quad (2.5.17)$$

Considering the gray-diffuse surface case, the spectral directional emissivity is equal to the hemispherical total emissivity, indeed:

$$\begin{aligned} \epsilon(T) &= \frac{E_e(T)}{E_b(T)} \\ &= \frac{\epsilon'_e(T) \int_0^\infty \int_0^{2\pi} \int_0^{\frac{\pi}{2}} I_b(\lambda, T) \cos\theta \sin\theta \, d\theta \, d\phi \, d\lambda}{E_b(T)} \\ &= \frac{\epsilon'_e(T) E_b(T)}{E_b(T)} = \epsilon'_e(T) \end{aligned} \quad (2.5.18)$$

this is due to the fact that the emissivity has not spectral and directional dependencies.

## 2.5.2 Absorptivity

The concept of absorption of radiation by a body has already been introduced and analyzed from an optical point of view. Here, it is quantitatively described using the developed theory of thermal radiation.

All the bodies do not only emit radiation, but they also absorb it. The surface radiative property that describes this behavior is the absorptivity,  $\alpha$ . It is a different scenario with respect to the one of emissivity. In that case, the aim is to quantify how much radiation is generated due to the surface temperature. Now, the goal is to study the reaction of the body to incident electromagnetic waves, such as light. It is a more complicated case because in addition to the surface temperature, the directions and wavelengths of the incident rays must be taken into consideration. Furthermore, the spectral distribution of incident radiation does not depend on temperature, *i.e.*, the radiation is itself temperature independent.

To understand and evaluate absorptivity, it is better to start again from the analysis of an incident wave on a surface. The power density of the incident radiation is: partially reflected, partially absorbed and partially transmitted. It is possible to summarize what has just been said with the following equation:

$$Q_{inc} = Q_{refl} + Q_{trans} + Q_{abs} \quad (2.5.19)$$

where  $Q$  is the rate of energy and has the dimension of power density, *i.e.*,  $\frac{W}{m^2}$ . Then, dividing all the terms by the incident power density:

$$\frac{Q_{inc}}{Q_{inc}} = \frac{Q_{refl}}{Q_{inc}} + \frac{Q_{trans}}{Q_{inc}} + \frac{Q_{abs}}{Q_{inc}} \quad (2.5.20)$$

Then, it can be rewritten as:

$$1 = \rho + \tau + \alpha \quad (2.5.21)$$

where  $\rho$ ,  $\tau$  and  $\alpha$  are the hemispherical total quantities of the reflectivity, the transmissivity and the absorptivity. Here, it is applied the same indication of the emissivity case. To simplify the previous equation, the concept of *opaque surface* is introduced, it is a surface that does not allow any radiation to pass through and so its transmittivity is equal to zero,  $\tau = 0$ . Then, the equation (2.5.23) becomes:

$$1 = \rho + \alpha \quad (2.5.22)$$

Or, reordering the terms:

$$\alpha = 1 - \rho \quad (2.5.23)$$

which provides an operative way of computing the absorptivity.

### 2.5.2.1 Directional spectral absorptivity

Another way to define absorptivity is the radiative perspective. The surface element  $dA_n$  absorbs the incident energy coming from the emitting area  $dA$  within the solid angle (Figure 2.6). This is evaluated by the integral along solid angle and wavelength of  $I_{\lambda,e}$ . Then, it can be defined as the ratio between the spectral radiation intensity absorbed by the surface and the one incident on it, it follows that the *spectral directional absorptivity* is:

$$\alpha'_{\lambda}(\lambda, T_a, \theta_i, \varphi_i) = \frac{\partial Q_{abs}(\lambda, T, \theta, \varphi)}{\partial A_i \cos \theta_i \partial \Omega_i \partial \lambda I_{\lambda,i}(\lambda, T_i, \theta_i, \varphi_i)} \quad (2.5.24)$$

it is a dimensionless quantity defined from 0 to 1.  $dQ_{abs}$  is the power absorbed, W, which depends on the absorption surface temperature,  $T_a$ . The main difference of this definition with respect to those pertaining the emissivity lies in the fact that the quantities at the denominator are related to the radiation incident on the object.

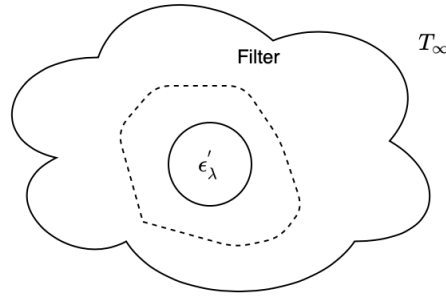


Figure 2.10: Object in a evacuated chamber surrounded by a filter

### 2.5.3 Kirchhoff's law

The equation (2.5.23) relates absorptivity, reflectivity and transmissivity, but the emissivity does not appear in this relation. The experiments analyzed in the black body section show that there is a relation between emissivity and absorptivity. It is possible to put up a conceptual experiment to understand this relation.

Consider the system depicted in figure (2.10), there is an object, represented by a circle, at initial temperature  $T_w$  within an isothermal evacuated chamber at temperature  $T_\infty$ , which is lower than the one of the object. As in the previous experiment on black body, neither conduction nor convection take place. The object, whose spectral directional emissivity is  $\epsilon'_\lambda(\lambda, T, \theta, \varphi)$ , is surrounded by a band-pass filter that allows only radiation with wavelengths in a small defined interval to pass. The one with any other wavelengths is back-reflected and absorbed by the body. Therefore, the object can reach the radiative-thermal equilibrium with the chamber by only emitting and absorbing electromagnetic waves in the wavelengths interval defined by the filter. It follows that spectral emissivity and spectral absorptivity of the object must be the same.

The same considerations can be applied to the directional case. Substituting the spectral filter with one that permits radiation only in one direction to pass, then directional emissivity and directional absorptivity must be equal.

Then, it is possible to make a more quantitative description of this experiment. First, the net power transfer between the two body is equal to the difference of outgoing and incoming rate of energy,  $W$ :

$$dQ_{net} = dQ_{outgoing} - dQ_{incoming} \quad (2.5.25)$$

Concerning the incoming radiation, it is simply the radiation incident on the object, then:

$$dQ_{incoming} = dQ_{incident} \quad (2.5.26)$$

About the outgoing radiation, the two sources are the emitted radiation and the radiation reflected by the object:

$$dQ_{outgoing} = dQ_{emitted} + dQ_{reflected} \quad (2.5.27)$$

Substituting:

$$dQ_{net} = dQ_{emitted} + dQ_{reflected} - dQ_{incident} \quad (2.5.28)$$

Now, recalling the equation (2.5.19) and assuming that the object has opaque surface,  $dQ_{trans}=0$ :

$$dQ_{incident} = dQ_{reflected} + dQ_{absorbed} \quad (2.5.29)$$

Replacing in (2.5.28):

$$dQ_{net} = dQ_{emitted} - dQ_{absorbed} \quad (2.5.30)$$

At the equilibrium the net heat transfer is equal to zero, so:

$$dQ_{emitted} = dQ_{absorbed} \quad (2.5.31)$$

The infinitesimal power emitted is identical to the infinitesimal power absorbed. Now, substituting the two terms with (2.4.11) and (2.5.24):

$$\begin{aligned} \alpha'(\lambda, T, \theta_i, \varphi_i) dA_i \cos\theta_i d\Omega_i d\lambda I_i(\lambda, T, \theta_i, \varphi_i) = \\ \epsilon'(\lambda, T, \theta_i, \varphi_i) dA_i \cos\theta_i d\Omega_i d\lambda I_b(\lambda, T) \end{aligned} \quad (2.5.32)$$

It is possible to assume that the isothermal evacuated enclosure behaves as a black body. So, it is a uniform and isotropic emitter, since it is much larger than the object and the wall are perfectly reflectors for radiation of any wavelengths. Furthermore, at equilibrium, the small object and the cavity are at the same temperature  $T$ . Then:

$$I_{\lambda, i} = I_{\lambda, b} \quad (2.5.33)$$

To maintain the equilibrium, the body has to emit radiation of the same intensity, at the same wavelength and direction.

Therefore, simplifying the equation (2.5.32):

$$\alpha'(\lambda, T, \theta_i, \varphi_i) = \epsilon'(\lambda, T, \theta_i, \varphi_i) \quad (2.5.34)$$

The emission and absorption spectrum of a body are identical, this is the most general representation of Kirchhoff's law, demonstrated in Planck's book [30]. It has been experimentally verified and the theoretical experiment used to reach this equation is an example of its validity.

This law gives the possibility to evaluate the emissivity from the equation (2.5.23) by using the Fresnel equation, which means that the emissivity of a material can be computed from its refractive index, as it will be shown in the next chapters.

# Chapter 3

## Radiative cooling

In this chapter, the radiative cooling mechanism based on the theory of radiative heating is examined and physically formulated. As a first step, a scenario where only the radiative cooler and atmosphere are present is analyzed, *i.e.*, *night-time radiative cooling*. Then, the Sun is added to the equation for a more realistic situation, *i.e.*, *day-time radiative cooling*. The heat transfer experiment between these actors has been done for different emissivity curves of the radiative cooler to better grasp the concept. This chapter is fundamental to build the basis for the model aimed at simulating its impact on the efficiency of a solar cell.

### 3.1 Night-time radiative cooling

A simple example of the radiative cooling mechanism that anyone can have in mind is frost: it appears during a clear night, even if the atmospheric temperature is above 0 °C. This phenomenon is strictly connected to the radiative heat transfer. Indeed, the ground faces the sky and constantly emits heat radiation towards it. Most of the emitted radiation is not absorbed or reflected by the atmosphere but directly goes to space. In other words, the atmosphere does not send it back to the surface.

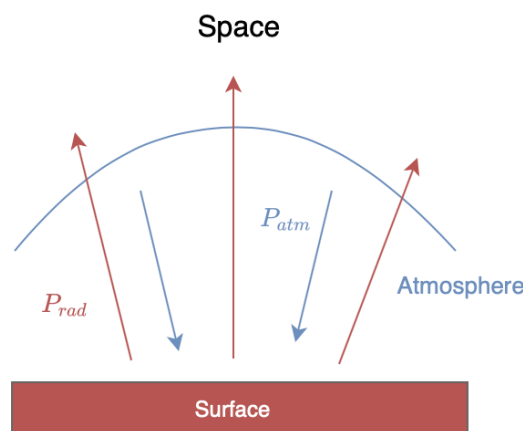


Figure 3.1: An ideal experiment of night-time radiative cooling mechanism

Thus, the surface of the field cools down and reaches a temperature below the freezing one. Then, the water vapor molecules in the air in contact with the ground solidify generating frost. The phenomenon at the base of frost generation is the so-called *night sky radiative cooling*.

To make this example clearer, it is necessary to study the heat fluxes between a surface and the atmosphere. The starting point is an ideal scenario where the object is modeled as a black body that exchanges heat *only* through radiation with the atmosphere (Figure 3.1). Later, the black body is replaced by an ideal emitter to highlight and exploit the radiative cooling mechanism.

The ideal experiment discussed and represented in figure (3.1) can be formulated by the *heat balance equation* [25], which reads:

$$P_{net}(T) = P_{rad,cooler}(T) - P_{atm}(T_{atm}) \quad (3.1.1)$$

where  $P_{rad}$  is the surface power density radiated by the surface and  $P_{atm}$  is the power density that it absorbs from the atmosphere. In this view, all the terms involved in (3.1.1) have dimension  $\frac{W}{m^2}$ .  $T_{atm}$  is the ambient temperature and corresponds to the one experienced by the human being. It is employed to compute  $P_{atm}$  because most of the *down-welling atmospheric long-wave radiation* absorbed by the surface comes from chemical compounds that are especially present near to the ground, such as water and carbon dioxide [35].

Equation (3.1.1) is written with respect to all the surface incoming and outgoing powers. The system reaches the equilibrium when the  $P_{net}$  is zero, this happens when the surface radiated and absorbed powers are identical.

In this regard, the heat balance equation (Eq. 3.1.1), and its extensions, is the fundamental tool for evaluating the impact of radiative cooling.

### 3.1.1 Atmosphere power density

Equation (3.1.1) involves the surface power density absorbed from the atmosphere,  $P_{atm}$ . Evaluating this contribution requires to introduce a number of preliminary concepts. The first is the transmission spectrum of the atmosphere, which is reported in figure (3.2).

Its profile is related to the different chemical elements in the atmosphere. For example, the peak at  $10\mu\text{m}$  is due to the absorptivity of the ozone ( $O_3$ ). It is important to have in mind that there are different factors that affect the transmissivity of the atmosphere, for example, the amount of water vapor [36], radiation direction or temperature. In this work, the models have been developed using the

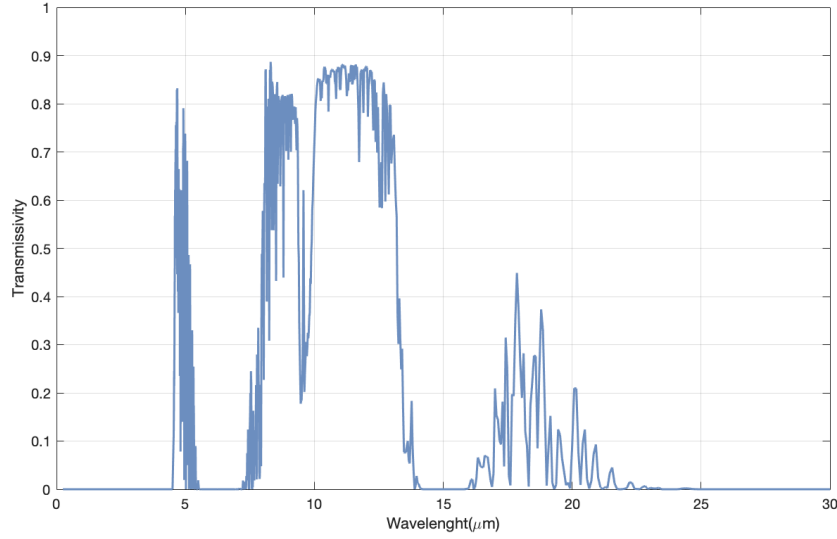


Figure 3.2: Spectral transmissivity of atmosphere at zenith

same atmospheric spectrum. The data of the transmission spectrum employed are taken from the RadCool simulation software [37], which are calculated by using the computational tool MODTRAN [38]. The first thing that one notices from the spectrum is that there are some ranges in which the transmissivity is high: in the mid-wavelength infrared region (MWIR) around  $5 \mu\text{m}$ , in the long-wavelength infrared region (LWIR), in particular from  $8$  to  $13 \mu\text{m}$ , and in the far infrared region (FIR), from  $16$  to  $24 \mu\text{m}$ . The second range is called *transparency window*. This spectral interval is interesting because it overlaps the peak of black body spectral emissivity curve at ambient temperature,  $T_{atm} = 300 \text{ K}$ , as it is shown in figure (3.3). Thus, the power radiated from the surface in this window propagates to the outer space without expiring significant absorption.

The total power per unit area absorbed by the surface from the atmosphere is expressed as:

$$P_{atm}(T_{atm}) = \int d\Omega \cos\theta \int_0^\infty I_{BB}(T_{atm}, \lambda) \epsilon(\lambda, \theta) \epsilon_{atm}(\lambda, \theta) d\lambda \quad (3.1.2)$$

where  $d\Omega$  is the solid angle (Eq. 2.4.4), sr,  $I_{BB}$  is the spectral radiation intensity of a black body, which is described by the Planck's law (Eq. 2.4.18),  $\frac{\text{W}}{\text{m}^2 \mu\text{m sr}}$ ,  $\epsilon(\lambda, \theta)$  is the absorptivity of the surface,  $\epsilon_{atm}(\lambda, \theta)$  is the emissivity of the atmosphere. It is important to notice that the absorptivity of the surface is indicated with the same symbol of the emissivity according to Kirchhoff's law (Eq. 2.5.34), which ensures that the absorptivity and emissivity are equal at equilibrium.

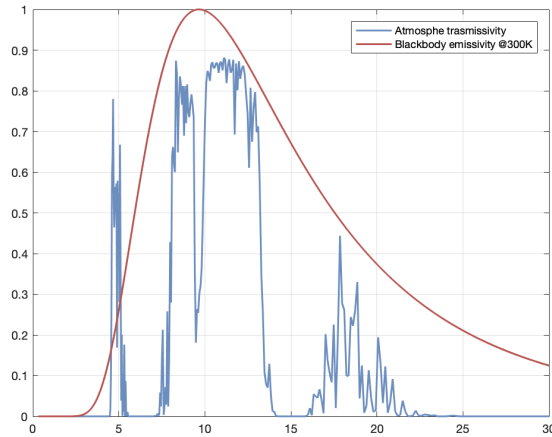


Figure 3.3: Superposition of the black body emissivity and atmosphere transmissivity

In this equation, it is multiplied by the emissivity of the atmosphere because the surface absorbs power only where they are both different from zero. In other words, absorptivity defines the quantity of the atmospheric emitted power absorbed by the surface.

The atmosphere is a gaseous envelope that radiates energy in every direction. For this work scope, it can be represented as a hemisphere surrounding the surface. Therefore, the solid angle is evaluated for the entire hemisphere (Eq. 2.4.5).

The angular dependence of the atmosphere emissivity can be evaluated starting from the spectral transmissivity at the zenith,  $\tau_{atm}(\lambda)$ , by the equation [39]:

$$\epsilon_{atm}(\lambda, \theta) = 1 - [\tau_{atm}(\lambda, 0)]^{\frac{1}{\cos\theta}} \quad (3.1.3)$$

This expression highlights the angular dependence, which is the most influencing factor with the humidity and cloud factor. The emissivity is lowest at the zenith,  $0^\circ$ , and highest at the horizon,  $90^\circ$ , (Figure 3.4).

Since the emissivity of the atmosphere is very complex, an angular-averaged emissivity is often used to reduce the computational burden. Recalling the hemispherical spectral emissivity equation (Eq. 2.5.9), it is possible to evaluate the average atmosphere emissivity as [35]:

$$\bar{\epsilon}_{atm}(\lambda) = 2 \int_0^{\pi/2} \epsilon_{atm}(\lambda, \theta) \cos\theta \sin\theta d\theta \quad (3.1.4)$$

where the angular dependence is eliminated. Eventually, the spectral radiation

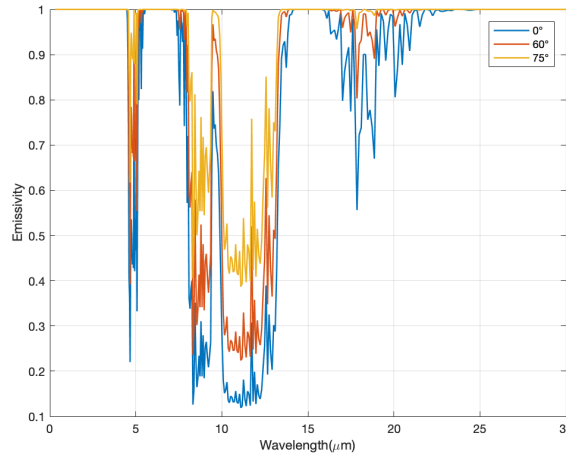


Figure 3.4: The atmosphere emissivity for three different polar angles

intensity of the atmosphere is defined as:

$$I_{atm}(T_{atm}, \lambda) = I_{BB}(T_{atm}, \lambda) \bar{\epsilon}_{atm}(\lambda) \quad (3.1.5)$$

Then, the equation (3.1.2) becomes:

$$P_{atm}(T_{atm}) = \int d\Omega \cos\theta \int_0^\infty I_{atm}(T_{atm}, \lambda) \epsilon(\lambda, \theta) d\lambda \quad (3.1.6)$$

where the only angle dependence term is the emissivity of the surface.

### 3.1.2 Surface power density

The second term that has to be calculated from the equation (3.1.1) is  $P_{rad, cooler}(T)$ . The power density radiated by the surface is defined as:

$$P_{rad, cooler}(T) = \int d\Omega \cos\theta \int_0^\infty I_{BB}(T, \lambda) \epsilon(\lambda, \theta) d\lambda \quad (3.1.7)$$

where  $I_{BB}$  is the spectral radiation intensity of the black body,  $\frac{W}{m^2 \mu m sr}$ , which depends on the surface temperature  $T$ , K,  $d\Omega$  is the solid angle, sr,  $\epsilon(\lambda, \theta)$  is the spectral and directional emissivity of the surface. The last parameter provides a degree of freedom to engineer the surface dielectric properties through the employment of metamaterials. This materials allow tailoring the directional and spectral emissivity of the surface through the design of nanostructures. Then, the possibility of controlling the emissivity enables the possibility to exploit radiative cooling mechanism, so that the engineered surface at ambient temperature emits radiation

stronger than the absorbed one. In this way, the material passively cools down below the ambient temperature. This can be employed in a lot of fields, such as air-conditioning systems.

The following sections present some emitter examples, and a comparison appraisal demonstrating the potential and limits of surface engineering. Since ideal cases have been analyzed, the *diffusive surface approximation* is employed for the analyzed emissivities.

### 3.1.2.1 Black body thermal emitter

The first emitter under study is the black body, which is a perfect emitter. The emissivity of a black surface is by definition isotropic and equal to one for every wavelength, as it is represented in figure (3.3). Thus, it is possible to rewrite the two terms of the heat balance equation as:

$$P_{atm}(T_{atm}) = \int d\Omega \cos\theta \int_0^\infty I_{atm}(T_{atm}, \lambda) d\lambda \quad (3.1.8)$$

$$P_{rad, cooler}(T) = \int d\Omega \cos\theta \int_0^\infty I_{BB}(T, \lambda) d\lambda$$

The thermodynamic equilibrium of the system is reached when the power radiated by the black body is equal to the absorbed one from the atmosphere. Obviously, the black body at ambient temperature emits more power than the one absorbed from the atmosphere. Then, its temperature decreases in order to balance the two powers. The ambient temperature does not change, it is constant at 300 K.

The objective of the study is to determine the black surface temperature  $T$  as the zero of the equation (3.1.1). From a mathematical point of view, this process can be seen as the variation of the areas subtended by the two integrals up to they correspond,  $P_{atm} = P_{rad, cooler}$ , (Figure 3.5). The temperature for which the net cooling power is equal to zero,  $P_{net} = 0$ , is called *equilibrium temperature*. The integrals were computed for the range of wavelength  $\lambda = 0.3 \div 250 \mu\text{m}$ , and the equilibrium is reached at the temperature of 281.67 K. Hence, the temperature surface is way below the ambient one, thanks to the radiative cooling mechanism. It fixes an upper bound for the temperature, *i.e.*, every object will reach a lower equilibrium temperature in this same conditions.

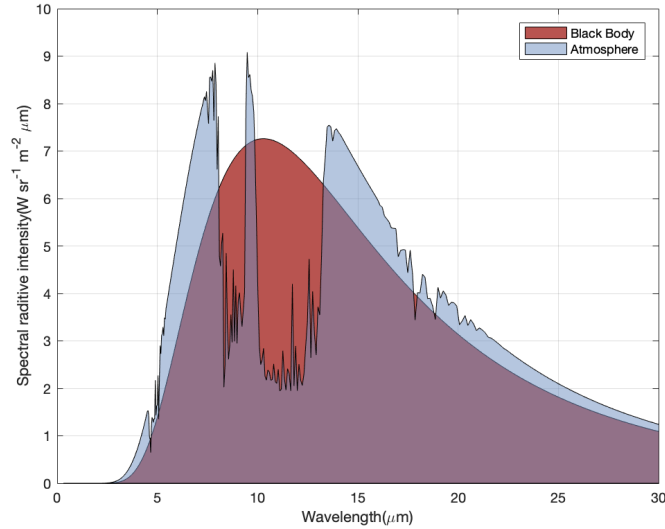


Figure 3.5: The spectral emissivity of black body and atmosphere at thermodynamic equilibrium

### 3.1.2.2 Optimal selective thermal emitter

The previous section presents the case of maximum coupling between atmosphere and emitter since the emissivity is constant. On the other hand, this section presents the other bound, *i.e.*, the optimal selective emitter. To this scope, the emissivity profile that minimizes the intersection of the two areas of the figure (3.5) for each temperature is looked for. This can be performed using the following expression [40]:

$$\epsilon_{ideal}(\lambda, T) = \frac{1}{2} [1 + \text{sgn}(I_{BB}(\lambda, T) - I_{atm}(\lambda, T_{amb}))] \quad (3.1.9)$$

where  $\text{sgn}(x)$  is the sign function, which reads:

$$\text{sgn}(x) := \begin{cases} -1 & \text{if } x < 0 \\ 0 & \text{if } x = 0 \\ 1 & \text{if } x > 0 \end{cases} \quad (3.1.10)$$

The idea behind the optimal selective emitter is: the emissivity is one where the spectral radiation intensity of the surface is greater than the one of the atmosphere, in any other case the emissivity is zero. In other words, the surface emits at a specific wavelength only if its power radiated is greater than the one absorbed, in this way it cools down. To make this concept clearer, figure (3.6) is reported,

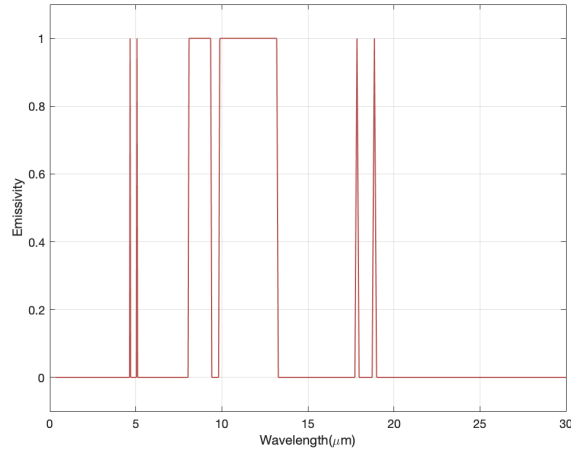


Figure 3.6: The spectral emissivity of an optimal selective emitter at the temperature of 281.67 K

it depicts the emissivity of an optical selective emitter at the equilibrium temperature of a black body emitter, using as reference the figure (3.5). Then, it can be seen that the emissivity is one in the whole transmission window except for the ozone absorption peak.

Differently from the previous cases, the emissivity depends on the surface temperature, so it has an optimal expression for any temperature. Indeed, it allows to compute the theoretical minimum temperature reachable by a surface by solving the heat balance equation with this emissivity. It has been found that  $T_{optimal,min}$  is equal to 217.7 K. For lower temperatures, the emissivity is equal to zero for any wavelength, that is, the radiative heat exchange between the atmosphere and surface does not occur anymore, and so it has no physical meaning.

### 3.1.2.3 Selective thermal emitter

The optimal selective emitter is a idealized model to obtain the best possible emissivity. Another interesting emissivity spectrum is a window function that is one in the transparency window and zero out of it (Figure 3.7). The surface reflects or transmits all the radiation at wavelengths outside the window. This is more realistic and suitable to be used as a benchmark for comparison with the real emissivity of material. The scientists aim to obtain this kind of spectrum, such as Raman et al. [25]. The selective thermal emissivity is defined as:

$$\epsilon(\lambda) := \begin{cases} 1 & 8 \mu\text{m} \leq \lambda \leq 13 \mu\text{m} \\ 0 & \text{others } \lambda \end{cases} \quad (3.1.11)$$

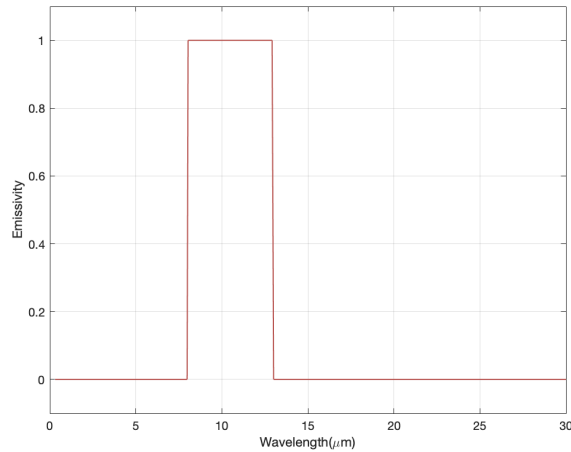


Figure 3.7: The spectral emissivity of a selective emitter

It depends only on the wavelength.

Here, it is important to discuss the influence of temperature on the object emissivity and explain why in the case of a selective emitter is not taken into account. One can think about the variation of the black body emissivity curve with the rise of temperature, that is, the peak of the spectral radiative intensity moves towards a smaller wavelength. Anyway, the modification of the emissivity curve is notable only for a large change of temperature [41]. Since in most of the radiative cooling applications the temperature range is not so wide, the emissivity is supposed to be independent of it [35].

The minimum temperature reached by this emitter is 248.6 K, which lies in be-

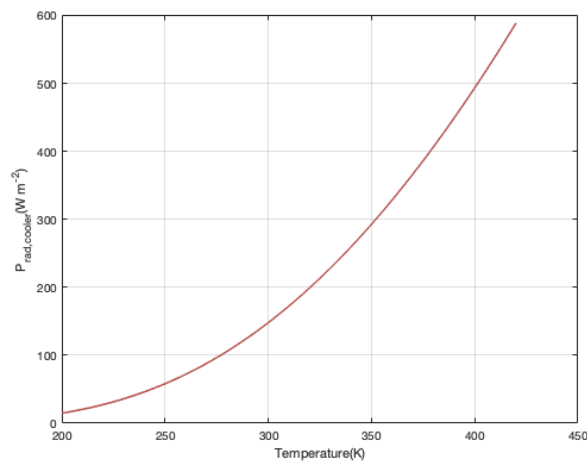


Figure 3.8: The power radiated by a selective emitter with respect to its temperature

tween the two previously obtained.

The figure (3.8) shows the power radiated by the selective emitter at different temperatures. According to the black body radiance (Eq. 2.4.18), it is proportional to the temperature. The emitted power increases with temperature. The equilibrium temperature of the radiative cooler corresponds to the one in which it emits enough power in order to balance all the absorbed ones, such as the power coming from the atmosphere.

### 3.1.3 Comparison between emitters

It is interesting to analyze the net cooling power density variation with respect to the temperature for each emitter. In order to do this the ambient temperature,  $T_{atm}$ , has been fixed to 300 K and the surface temperature,  $T$ , has been varied in a range from 200 to 300 K. In the abscissas is reported the difference between the two temperatures,  $T - T_{atm}$ , to assess the effectiveness of the emitter as a cooling device. It has to be remarked that most significant points are the one in which the net cooling power reaches zero, it defines the temperature at equilibrium. The cooling power behavior of emitters is reported in figure (3.9). As expected, the optimal selective emitter has the best performance and the black body emitter the worst. Hence, their equilibrium temperatures identify an interval that includes all the possible radiative cooler performances.

The net cooling power provided by the selective emitter is higher than the black

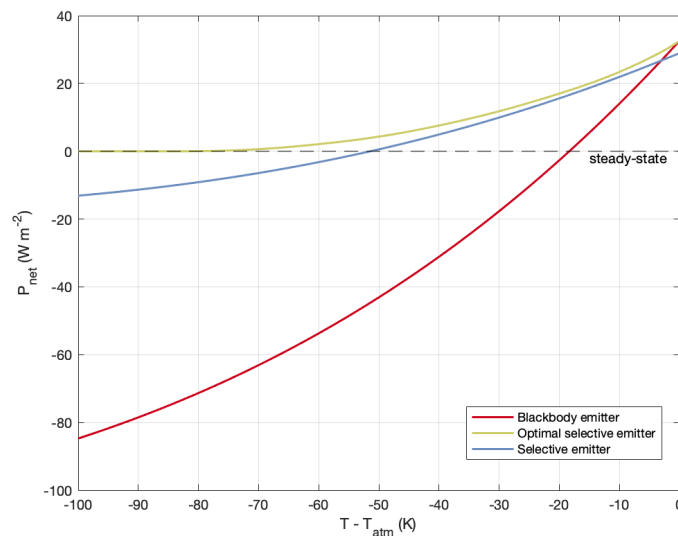


Figure 3.9: The comparison among net cooling power of different emitters

body one since it enhances the radiative cooling mechanism of the surface. The optimal selective emitter curve behaves similarly to the selective emitter one for temperature closer to the ambient one, *i.e.*, the two emissivities have comparable profiles. Then, the curve goes to zero. The only zero that has physical meaning is the first one encountered going from 0 to  $-100\text{ K}$ ,  $T_{optimal,min}$ . From this temperature, the net power exchange does not occur anymore due to the emissivity definition [40].

The net cooling power is negative when the surface radiates less power than the absorbed one, so its temperature has to increase to reach the radiative equilibrium. The opposite happens when the net cooling power is greater than zero. This term is used to compare different thermal emitters because it evaluates their cooling performance at any surface temperature.

## 3.2 Day-time radiative cooling

The previous discussion is focused on night-time radiative cooling, which is characterized by having no contribution from the Sun. But, most of the applications are requested during the day, leading to the need to study also *day-time radiative cooling*. The scope of this section is to estimate its contribution to the heat balance equation. This will be useful in the next chapters, to evaluate the impact of the radiative cooler on solar cell efficiency. The heat balance equation that describes this system is the (3.1.1) with an additional negative power term, which takes into account the Sun influence:

$$P_{net}(T) = P_{rad,cooler}(T) - P_{atm}(T_{atm}) - P_{sun} \quad (3.2.1)$$

where  $P_{sun}$  is the power density absorbed by the radiative cooler from the Sun,  $\frac{\text{W}}{\text{m}^2}$ .

Considering the solar spectra in figure (1.3), it is clear that the radiation coming from the Sun is mainly concentrated in the wavelength interval from  $0.3$  to  $2.5\ \mu\text{m}$ . This characteristic of the spectrum must be considered for the development of materials based on the day-time radiative cooling mechanism. The radiative cooler has to be a reflector or transmitter in this range of wavelength. In most cases, it has high reflectance outside the emissivity range, for example, if it is employed to cool down the water in an air-conditioning system, it will be a reflector for the solar radiation. From another point of view, the solar power incident on a radiative cooler on the ground is about  $1\ \frac{\text{kW}}{\text{m}^2}$ . The net cooling power of a selective

emitter at 300 K is about  $30 \frac{\text{W}}{\text{m}^2}$ . Then, it has to reflect more than 97% of solar radiation to behave as a cooling device.

The day-time radiative cooling requires the control of the material optical properties in a wide range of wavelengths. The most important parameters for the design of a radiative cooler are thermal emissivity and solar reflectivity.

### 3.2.1 Solar power density

The total power per unit area absorbed by the surface from the sun is calculated as:

$$P_{sun} = \cos\theta_{sun} \int_0^{\infty} AM1.5g(\lambda)\epsilon(\lambda,\theta_{sun})d\lambda \quad (3.2.2)$$

where  $AM1.5g$  is the spectral solar irradiance,  $\frac{\text{W}}{\text{m}^2\text{nm}}$ ,  $\theta_{sun}$  is the angle between the normal of surface and the solar incident radiation, rad,  $\epsilon$  is the surface absorptivity in according to the (2.5.34). Usually, it is assumed that the surface is facing the sky at a fixed angle, which is the zenith, so that there is no angular integral in the equation (3.2.2). This approach is used even in other publications, such as [25] and [35]. Therefore, the above equation is rewritten for  $\theta_{sun}=0$  as:

$$P_{sun} = \int_0^{\infty} AM1.5g(\lambda)\epsilon(\lambda,0)d\lambda \quad (3.2.3)$$

the surface emissivity is defined only for the zenith.

This term will become important when the structure with a real emissivity will be analyzed.

# Chapter 4

## The impact of a radiative cooler on solar cell

In this chapter, the effectiveness of the radiative cooler as a passive cooling device for the solar cell is analyzed. To this scope, an approach similar to the one presented in Chapter 3 is used. A new heat balance equation of the system is formulated, including also the power density contribution of the non-radiative heat transfer mechanisms and the solar cell, which description is based on the model of Shockley and Queisser developed in Chapter 1. Then, the thermal model is tested through the reproduction of results available in the scientific literature. Several solar cell figures of merit are examined to show the impact of a ideal radiative cooler on it. In the end, an electromagnetic model based on the transmission line technique is used to investigate the optical properties of some multilayer structures. Then, the computed emissivities are fed to the thermal model to evaluate their impact on solar cells efficiency.

### 4.1 Thermal model

#### 4.1.1 Heat balance equation

The device under test is composed of a solar cell above a radiative cooler with a mirror on the rear (Figure 4.1). According to the solar cell structure studied in Chapter 1, a mirror is employed in the back of the structure. Its role is to increase the efficiency of the solar cell, but on the other hand, it reduces the impact of the radiative cooler. Indeed, if it emits in the two hemispheres, the power radiated by the cooler will be doubled. This structure has been designed and employed in different models [26, 42, 43]. It is interesting to notice that the radiative cooler position depends on its electromagnetic behavior. The power non-absorbed by the radiative cooler is transmitted or reflected. In the first case, the radiative cooler can be placed above the solar cell or between the mirror and the cell without changing the radiative behavior of the structure. In the latter

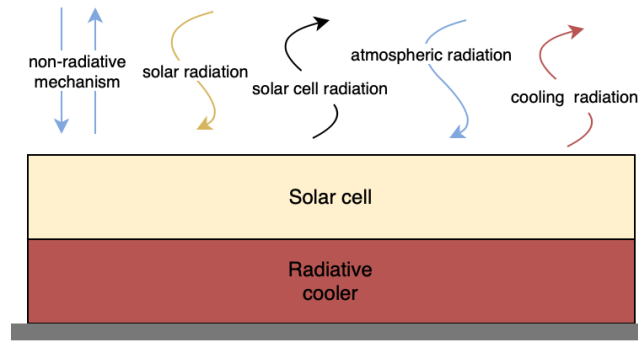


Figure 4.1: Radiative and non-radiative behaviour of a solar cell coupled to a radiative cooler

case, the structure works properly only with the radiative cooler below the solar cell. However, an ideal radiative cooler is considered in this chapter, then, the only important parameter is its emissivity. The device lies on the ground in contact with an external surface, surrounded by the atmosphere and under 1-sun of illumination<sup>1</sup>. Then, it is subjected to the non-radiative heat transfers, *i.e.*, thermal conduction and convection.

The power exchanges of the structure is described by the following heat balance equation:

$$P_{net}(T,V) = P_{rad,cooler}(T) + P_{conv,cond}(T,T_{atm}) - P_{atm}(T_{atm}) - P_{solar,heat}(T,V) \quad (4.1.1)$$

where  $P_{conv,cond}$  is the non-radiative power density,  $P_{solar,heat}(T,V)$  is the part of solar power absorbed that has to be dissipated by the radiative cooler and the convection and conduction mechanisms. It is computed as:

$$P_{solar,heat}(T,V) = P_{sun} - P_{electrical}(T,V) - P_{rad,cell}(T,V) \quad (4.1.2)$$

where  $P_{electrical}$  is an electrical power density,  $P_{rad,cell}$  is the power density radiated by the solar cell. The measurement unit of all the terms in equation (4.1.1) is  $\frac{W}{m^2}$ . The  $P_{solar,heat}$  corresponds to the power absorbed from the Sun that is converted into heat through the thermalization process. Then, the temperature of the solar cell increases. The radiative cooler limits the rise of this temperature helping the convection and conduction mechanisms to dissipate the heat, improving the radiative behavior of the system in the LWIR region.

At this point, it is interesting to notice that the power terms related to the radiative

<sup>1</sup>it is a way to measure of the light solar intensity on a cell, it corresponds to  $1 \frac{kW}{m^2}$ , which is obtained integrating the AM1.5g spectrum for all the wavelength.

cooler and the solar cell can be studied independently. They are only connected by the device temperature  $T$ , which is assumed to be uniform at every point of the structure. It is possible to say that they are independent from the radiative point of view, *i.e.*, they emit and absorb radiation in a different part of the spectrum. More precisely, the radiative cooler emits in the LWIR region, instead, the solar cell absorbs radiation in the range  $0.3 \div 4 \mu\text{m}$ , that is, for wavelengths shorter than  $\frac{hc}{E_g}$ .

Moreover, the atmospheric transmission spectrum is mostly concentrated in the Mid-wavelength infrared and Long-wavelength infrared regions [44]. In the range of the solar spectrum, the power absorbed by the photovoltaic modules from the atmosphere is negligible compared to the one absorbed by the radiative cooler [42]. Then, it is neglected in equation (4.1.1).

The emissivity profile of the radiative cooler considered is the one of a selective emitter, *i.e.*, it is equal to one from 8 to  $13 \mu\text{m}$  and zero out of it. The terms related to it are evaluated as in Chapter 3, that is,  $P_{rad,cooler}$ ,  $P_{atm}$  and  $P_{sun}$  are computed with equations (3.1.7), (3.1.2) and (3.2.2) respectively. Since the radiative cooler has ideal emissivity, it does not absorb power from the Sun. The emissivity of the equation (3.2.2) corresponds to the absorptivity of the solar cell. The other terms are introduced in the following sections.

### 4.1.2 Electrical power density

Assuming that the solar cell is constantly connected to an optimal load, the electrical power term is equal to the maximum power density of a solar cell (Eq. 1.4.35), then:

$$P_{electrical}(Eg,T) = J_{MPP}(Eg,T)V_{MPP}(T) \quad (4.1.3)$$

its unit is  $\frac{\text{W}}{\text{m}^2}$ .

It is interesting to analyze the temperature dependence of this term, which is directly connected to the efficiency of a solar cell. The electrical power of a solar cell decreases linearly with the rise of operating temperature (Left figure 4.2), because of the reduction of the open-circuit voltage. In other words, the rise of cell temperature causes the growth of the number of electrons that jump in the conduction band and recombine emitting photons, *i.e.*, the radiative recombination process increases (Right figure 4.2).

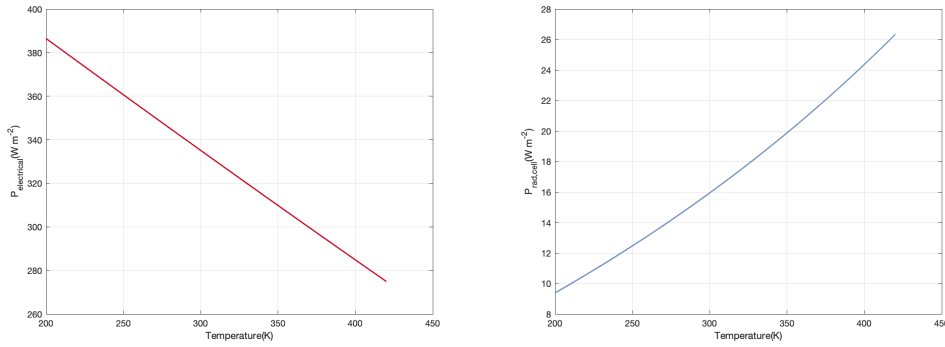


Figure 4.2: Left: the electric power density of a solar cell with  $E_g = 1.12$  eV with respect to the temperature. Right: The power radiated by a solar cells  $E_g = 1.12$  eV with respect to the temperature.

### 4.1.3 Radiated power density

The radiated power density is evaluated as in equation (4.1.5), then:

$$P_{r,0}(E_g, T) = E_g \int_0^{\infty} \alpha(E, E_g) \phi_E^e(E, T) dE \quad (4.1.4)$$

It is assumed that the solar cell works at the maximum power point, so the radiated power density in out of equilibrium conditions is evaluated:

$$P_{rad,cell}(E_g, T) = P_{r,0}(E_g, T) e^{\frac{V_{MPP}}{V_T}} \quad (4.1.5)$$

its unit is  $\frac{W}{m^2}$ .

### 4.1.4 Convection and conduction power

In addition to radiative heat transfer, the structure is directly in contact with air and an external surface, and thus influences the temperature of the structure through conduction and convection heat transfer mechanisms. Instead of using complex thermal simulators to evaluate the non-radiative heat transfers [26], it is possible to describe this thermal loss mechanism by a suitable coefficient and assuming that the temperature of the cell is uniform. Then, the power density loss due to conduction and convection is computed as [35, 43]:

$$P_{conv,cond}(T, T_{atm}) = h_c(T - T_{atm}) \quad (4.1.6)$$

where  $h_c$  is the *non-radiative heat transfer coefficient* that considers the combined effect of convective and conductive heating, it is expressed as:

$$h_c = h_{cond} + h_{conv} \quad (4.1.7)$$

its unit is  $\frac{W}{m^2K}$ .

This coefficient has been studied a lot in the past years, and it is usually computed by empirical formulas, such as [45]:

$$h_c = 2.8 + 3u_a \quad (4.1.8)$$

where  $u_a$  is the wind velocity, m/s. In this work, the value of the non-radiative heat transfer coefficient is computed for wind velocities from 1 to 3 m/s, which corresponds to the usual outdoor condition [46]. Then, the  $h_c$  varies from 5.5 to 12  $\frac{W}{m^2K}$ . The wind is the most significant heat loss factor for a solar cell. It is interesting to analyze the behavior of this term with respect to the temperature (Figure 4.3). The power is equal to zero if the cell has the same temperature as the ambient, therefore, it does not contribute to the heat balance equation, *non-radiative thermal equilibrium*. This power density is negative for temperatures below  $T_{atm}$ , *i.e.*, the non-radiative mechanisms heat the cell. It is positive for temperature above  $T_{atm}$ , so they help the radiative cooler to cool down the structure. The three heat transfer mechanisms work together to reduce the temperature of the solar cell. If only the radiative cooler is considered, the convection and conduction mechanisms will increase its equilibrium temperature, worsening its performe.

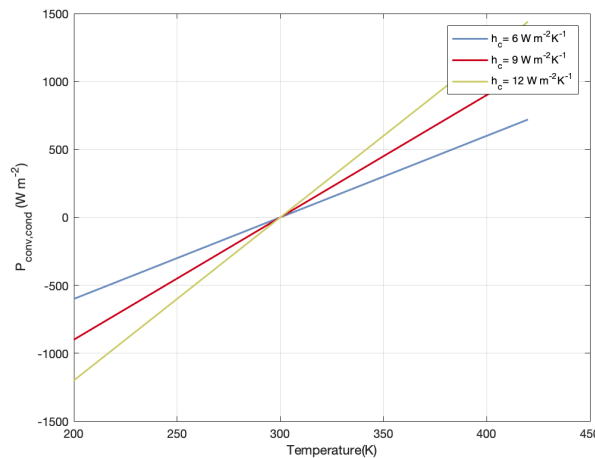


Figure 4.3: The conduction and convection power density for different  $h_c$  with respect to the temperature ( $T_{atm}=300 \text{ K}$ )

## 4.2 Results

This section is dedicated to the validation of the model and the results analysis. First, the comparison between the model developed in this work and a similar one present in scientific literature is reported. The absence of the non-radiative heat transfer term is the main difference between these two model, *vacuum condition*. The test is done for the terrestrial and extraterrestrial environment. Second, the comparison between different figures of merit of a solar cell with and without radiative cooler in typical condition is shown. At the end of the section, the electromagnetic model based on the transmission line technique for the computation of dielectric properties of multilayer structures is tested. Then, the computed emissivity is fed to the thermal model and a comparison between the realistic radiative cooler and ideal selective emitter is carried out.

### 4.2.1 Vacuum

The test of the model is done taking as reference the paper of Taqiyyah S. Safi and Jeremy N. Munday [42]. To this scope, the model is adapted to the simulating condition described in the paper for the terrestrial and extraterrestrial environment.

#### 4.2.1.1 Terrestrial environment

The structure is composed as the one in figure (4.1). But in this case, it is encapsulated in a vacuum chamber to eliminate the influence of the non-radiative heat transfer mechanisms. This does not affect the radiative behavior of the device. Then, the equation (4.1.1) becomes:

$$P_{net}(T,V) = P_{rad,cooler}(T) - P_{atm}(T_{atm}) - P_{solar,heat}(T,V) \quad (4.2.1)$$

plugging the equation (4.1.2):

$$P_{net}(T,V) = P_{rad,cooler}(T) - P_{atm}(T_{atm}) - P_{sun} + P_{electrical}(T,V) + P_{rad,cell}(T,V) \quad (4.2.2)$$

In these conditions, the heat generated by the thermalization process is dissipated *only* through thermal radiation. The radiative cooler emissivity is one from 8 to

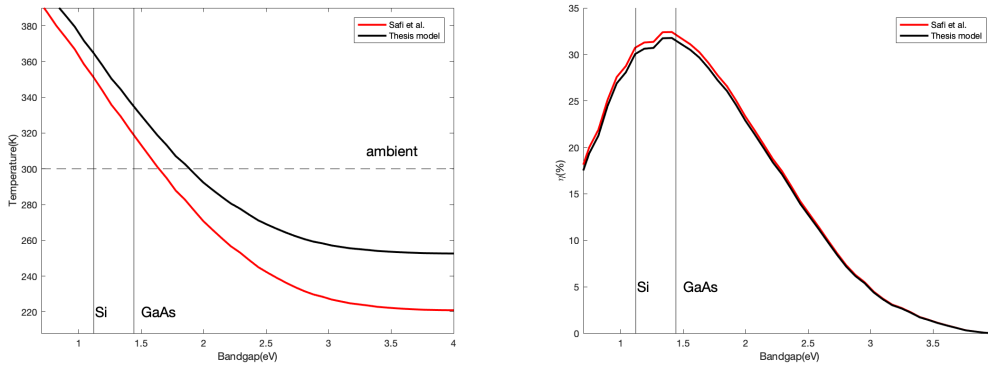


Figure 4.4: Left: The operating temperature with respect to the energy gap. Right: The efficiency with respect to the energy gap.

26  $\mu\text{m}$  and zero out of it. The absorptivity of the cell corresponds to the one considered in the thesis. In this computation, the data of the atmosphere transmission spectrum is taken from the Gemini Observatory website [36]. They correspond to the one in Mid-IR for water vapor column level of 5 mm, while the air mass is not specified. The transmissivity of the atmosphere strongly depends on the environmental condition considered. Then, it is mandatory to use the same spectrum to do a correct comparison between the results. Finally, the temperature for  $P_{net} = 0$  is computed.

In figure (4.4) are reported the simulation outcomes compared to the one obtained in the paper. From the figures, it is possible to do some consideration about the validation of the model. First, the red and black curves have similar behavior in both figures. Second, the operating temperature values reported by the black curve make sense considering the operating condition of the device. In other words, the radiative cooler effect is clear since the structure temperature is lower than the ambient one for energy gap above 1.91 eV, this would be not possible without it. Moreover, the efficiency values are comparable to the one of a solar cell working in typical operating condition, *i.e.*, at temperature of 335 K (Left figure 1.21). Then, if the non-radiative term is included in the computation, the solar cell with radiative cooler will work at a lower temperatures, which is the scope of the studied structure. Third, the difference between the two curves is related to the atmospheric term. The authors do not explain clearly how the atmospheric data are processed. In particular, they do not mention whether any pre- or post-processing elaboration or integration method is employed. Furthermore, the results obtained in the extraterrestrial case,  $P_{atm} = 0 \frac{\text{W}}{\text{m}^2}$ , are identical to the paper one.

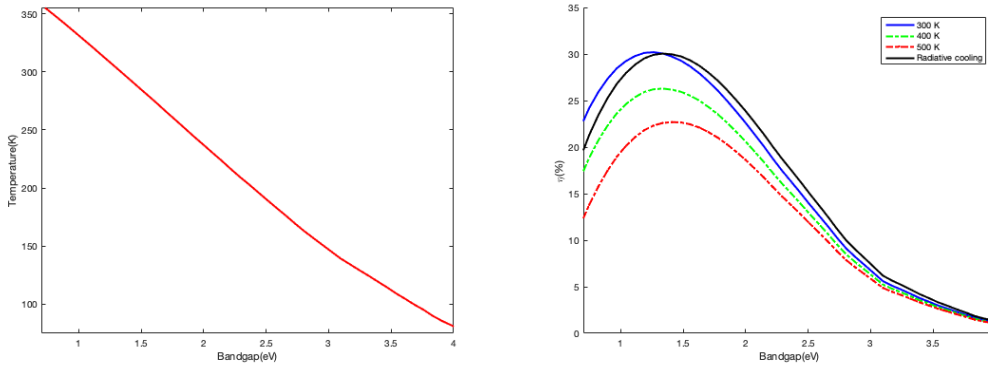


Figure 4.5: Left: The operating temperature with respect to the energy gap. Right: The efficiency with respect to the energy gap.

#### 4.2.1.2 Extraterrestrial environment

Since there is non-atmosphere in the space, the selective emitter is substituted by a black body emitter, which radiates more power. The cell is constantly oriented towards the Sun so that the black body emitter is screened from the solar radiation, moreover, the mirror is moved between the solar cell and the radiative cooler for the same scope. The NREL AM0 spectrum is employed in this computation (Sec. 1.4.0.1). In this view, the equation (4.2.2) becomes:

$$P_{net}(T,V) = P_{rad,cooler}(T) + P_{electrical}(T,V) + P_{rad,cell}(T,V) - P_{sun} \quad (4.2.3)$$

The results obtained are shown in figure (4.5), they are practically identical to the one obtained by Taqiyyah S. Safi and Jeremy N. Munday.

In this case, the solar cell with a radiative cooler has greater efficiency than a solar cell at 300 K for energy gaps higher than 1.34 eV. Then, the effect of the radiative cooler on the performance of the solar cell is evident. For example, the typical operating temperature of a silicon solar cell in a low-Earth orbit (LEO) is 328.5 K [47]. It decreases of 7.5 K in the radiative cooler application, which means an increase of the efficiency of 0.4%. Moreover, the PV models with an energy gap greater than silicon can reach an efficiency increment up to 2.6% considering the typical operating temperature reported in [47]. Since the radiative cooler is a perfect emitter, it has a better performance compared to the terrestrial case. Its effectiveness still increases, if it is employed in near-Sun mission in which the solar cells work at higher temperatures.

## 4.2.2 Atmosphere

The model comprehensive of the non-radiative power term is further validated with results available in scientific literature, in particular, the one obtained by Perrakis *et al.* [43] and Raman *et al.* [26].

At this point, the comparison between different figures of merit of a solar cell with radiative cooler and without is reported and examined. The first one is described by the equation (4.1.1). Whereas, the heat balance equation of the solar cell is:

$$P_{net,cell}(T,V) = P_{conv,cond}(T,T_{amb}) - P_{solar,heat}(T,V) \quad (4.2.4)$$

recalling that

$$P_{solar,heat}(T,V) = P_{sun} - P_{electrical}(T,V) - P_{rad,cell}(T,V) \quad (4.2.5)$$

The heat generated through thermalization is dissipated *only* through the convection and conduction mechanism. Here, the atmospheric spectrum employed is the one reported in Chapter 3. The radiative cooler is a selective emitter with emissivity equal to one from 8 to 13  $\mu\text{m}$ . Then, it does not absorb any radiation from the Sun but only from the atmosphere.

### 4.2.2.1 Net cooling power

First, it is interesting to study the variation of the net cooling power with respect to the non-radiative heat coefficient and temperature. The first thing to notice in figure (4.6) is the points of intersection between the black line and the other lines. They correspond to the steady-state points, i.e., the structure is in thermodynamic equilibrium,  $P_{net} = 0 \frac{\text{W}}{\text{m}^2}$ , and its temperature is  $T$ . For instance, the operating temperature of a silicon solar cell with a radiative cooler is about 325.7 K. Another interesting fact is the operating temperature difference of the two devices working in the same weather condition. This difference varies with the combined convection-conduction heat coefficient, which means that the radiative cooler impact decreases with the increasing of this coefficient. For example, for  $h_c = 12 \frac{\text{W}}{\text{m}^2\text{K}}$  the difference is 13.8 K, for  $h_c = 9 \frac{\text{W}}{\text{m}^2\text{K}}$  the difference is 20.9 K.

The crossing points at  $T - T_{atm} = 0 \text{ K}$  indicates that the structure is at non-radiative thermal equilibrium with the ambient. It is important to not confuse it

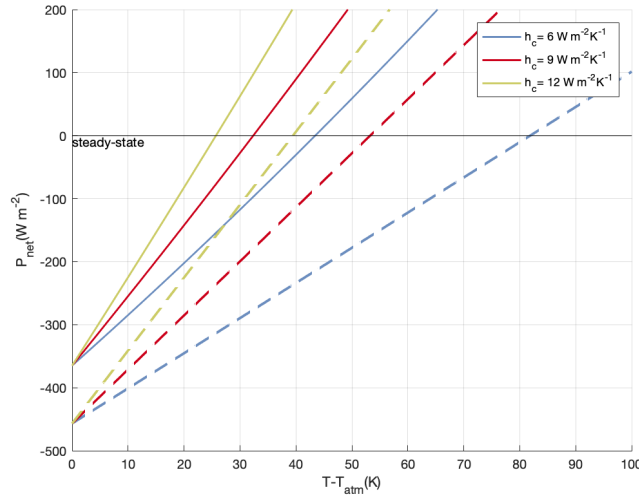


Figure 4.6: Net cooling power for different non-radiative coefficients with respect to the operating temperature ( $T_{atm} = 300$  K,  $E_g = 1.12$  eV), solar cell with radiative cooler (line), solar cell (dashed line).

with the thermodynamic equilibrium, which corresponds to the radiative and non-radiative thermal equilibrium, *i.e.*, the structure is in steady-state condition. However, the two points do not match since the radiative cooler increases the net cooling power of the structure. Indeed, this difference corresponds to  $P_{rad,cooler} - P_{atm}$ , which is about  $96 \frac{\text{W}}{\text{m}^2}$ . The variation of the net cooling power to temperature is linear but it has different slope for each non-radiative coefficient, *i.e.*, for higher values of  $h_c$  the line is steeper. Then, the structure at 300 K reaches a lower temperature when the wind velocity is higher, and in the case with the radiative cooler. For example, the slope of the solar cell with radiative cooler is equal to:  $10.2 \frac{\text{W}}{\text{m}^2\text{K}}$  for  $h_c = 9 \frac{\text{W}}{\text{m}^2\text{K}}$ ,  $13.2 \frac{\text{W}}{\text{m}^2\text{K}}$  for  $h_c = 12 \frac{\text{W}}{\text{m}^2\text{K}}$ .

#### 4.2.2.2 Operating temperature

The structure reaches the equilibrium for a certain operating temperature. The figure (4.7) reports the variation of this temperature for different crystalline solar cells. One can note that a c-Si solar cell works at 13.8 K lower with the radiative cooler. The structure temperature decreases at higher energy gaps. The solar cell absorbs less and less power from the Sun since the number of photons reduces at higher energy, consequently, the thermalization loss reduces and so does the heat that the structure has to dissipate,  $P_{solar,heat}$ . In the solar cell case, for an energy gap greater than 3.5 eV the power absorbed from the Sun is practically zero, hence, the solar cell is in thermal equilibrium with the ambient. The conduction

and convection mechanism maintains the temperature constant at 300 K. It is

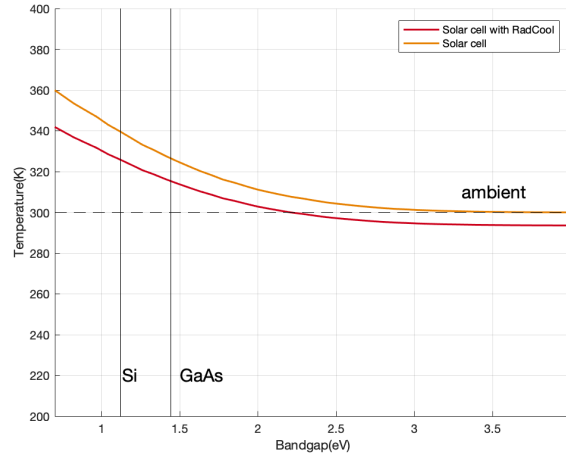


Figure 4.7: The variation of the operating temperatures with respect the energy gap with  $h_c = 12 \frac{\text{W}}{\text{m}^2\text{K}}$ .

interesting to notice the different behavior of the two curves. For temperature below the ambient one, the non-radiative heat transfer mechanisms heat up the structure limiting the effect of the radiative cooler. Graphically, the red curve moves closer to the yellow curve with the increase of temperature.

#### 4.2.2.3 Efficiency

In figure (4.6), it is possible to see the impact of the radiative cooler on the solar cell efficiency. It is higher for every energy gap up to 2 eV since the temperature gap reduces with the increasing of the energy gap (Figure 4.7). The maximum difference of the efficiency is reached for  $E_g$  lower than 1 eV. However, it is significant the result obtained for the silicon solar cell, the efficiency is 0.72% higher than the case in which only the solar cell is considered. This enhancement of the efficiency is computed without considering non-radiative recombination processes that occur in the solar cell. These recombination processes, such as Auger and Shockley-Read-Hall (SRH), are stronger than the radiative one and become significant at higher temperatures. Then, the impact of the radiative cooler is underestimated with this considerations. The 0.7% increase in solar cell efficiency is a remarkable achievement considering the impact on overall energy production. In the end, it is important to recall that these results are obtained for specific weather conditions represented by the atmosphere spectrum in Chapter 3, and with a selective cooler that exploits the only atmospheric window available. Substituting one of them or both, the results can noticeably change. For example, if

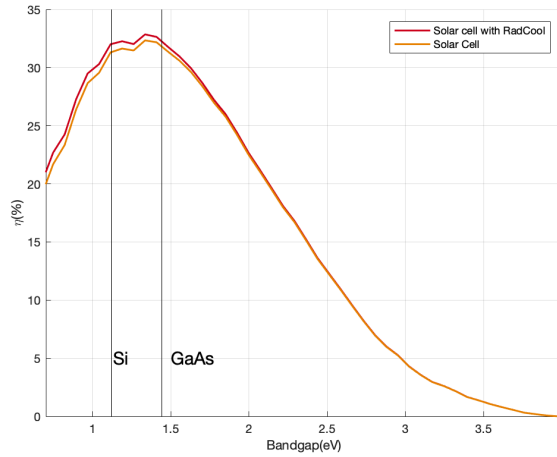


Figure 4.8: The variation of the efficiency with respect the energy gap with  $h_c = 12 \frac{\text{W}}{\text{m}^2\text{K}}$ .

the atmospheric spectrum and the selective emitter described in the paper of Safi *et. al* are used [42], the efficiency improvement will be higher. This result is due to the exploitation of the higher transmissivity of the atmosphere spectrum by the radiative cooler and a better transmissivity of the atmosphere.

### 4.2.3 Towards realistic radiative coolers

Here, the model presented in the previous section is employed to evaluate and examine the impact of more realistic photonic coolers on solar cell conversion efficiency. To compute the dielectric properties of two-dimensional multilayer structures an electromagnetic model based on the transmission line technique is developed [33]. This model is able to characterize the electromagnetic behavior of stratified structures by considering thickness, refractive index, and incidence angle as input. First, the model validation is done using some structures available in scientific literature. Then, the computed emissivity is used in the thermal model to evaluate its impact on the solar cell performance and do a comparison with the ideal case.

#### 4.2.3.1 Emissivity of photonic structures

The test of the model is done by taking as reference the structures presented in the paper of M.A. Kecebas *et al.* [48]. The first structure considered is the one reported in the left figure (4.9). The four layers of silicon and titanium dioxide starting from the bottom optimize the solar reflection of the structure, behaving

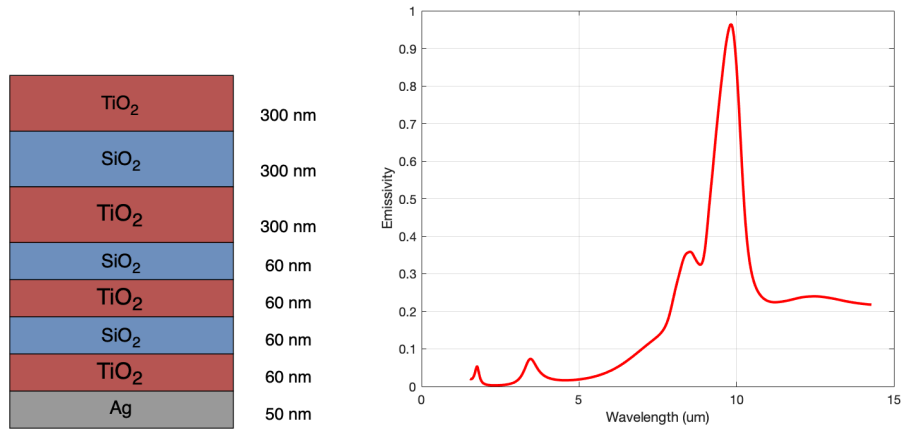


Figure 4.9: Left: Photonic structure composed of six layers of SiO<sub>2</sub>, three layers of SiO<sub>2</sub> and one layer of Ag. Right: Spectral emissivity of the implemented structure for incident angle of 0°.

like periodic structures. The thin layer of silver reflects the remainder of energy avoiding the parasitic absorption by the supporting structure. The thicker layers represent the absorption segment of the structure since they are primarily responsible for the thermal emission in the mid-IR region. In right figure (4.9) is reported the spectral emissivity of the structure for normal incidence. The dioxide refractive indices values have been taken from the article of Kischkat *et al.* [49], while the refractive index of silver from the article of Yang *et al.* [50]. This emissivity is very similar to the one obtained in the considered paper. The small differences are related to the different refractive indices values employed. It is important to notice the strong wavelength depends on the emissivity, it is related to the number of layers, incident angle, refractive index, and thickness. The thermal emission of this structure has to be enhanced, by changing one or more of these parameters, to improve the cooling performance of the photonic structures.

Hence, the structure design is changed, and a material with high emissivity in the range from 8 to 13  $\mu\text{m}$  is added. The thickness of the four thinner layers is reduced from 60 to 20 nm without influencing the reflectivity of the material [48]. The absorption segment is tripled, and their thickness is reduced from 300 to 200 nm. Moreover, the TiO<sub>2</sub> layer on top of the three segments is substituted by an Al<sub>2</sub>O<sub>3</sub> layer, which has stronger absorption in the atmospheric window compared to the other employed materials and does not absorb radiation at shorter wavelengths (Figure 4.10, a). This design increases considerably the emission of the structure, in particular, the one with the aluminium oxide has higher emissivity in mid-IR

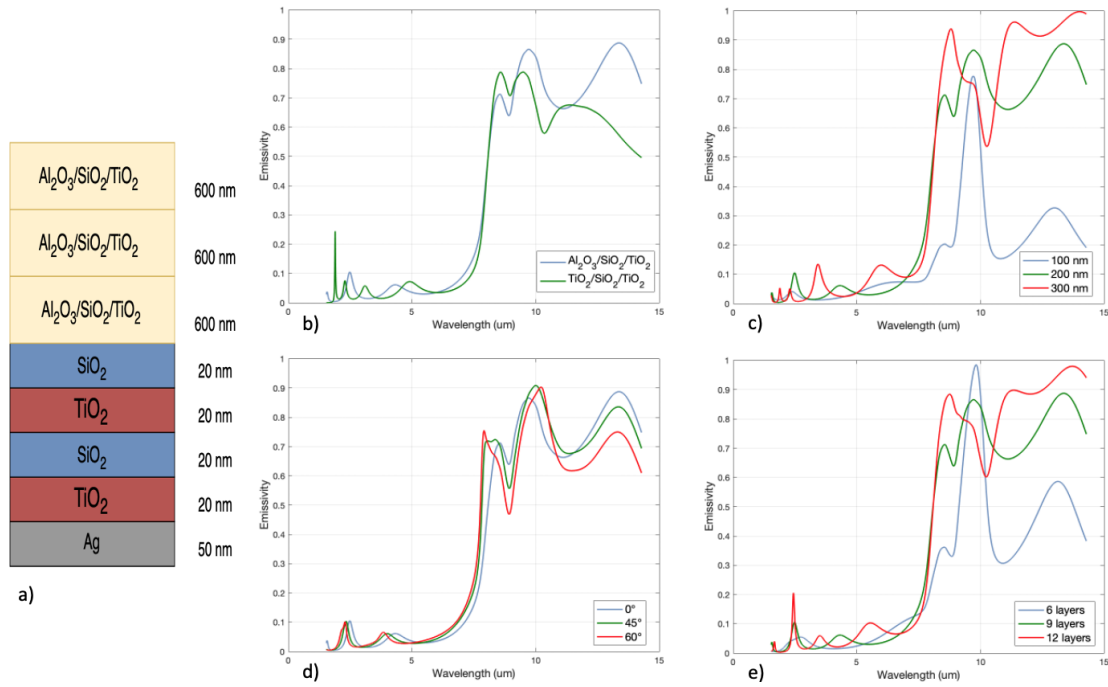


Figure 4.10: a) Multilayer structure under analysis. b) Emissivity comparison between two structures composed of different materials. c) Emissivity comparison of the same structure with different thicknesses of segment layers. d) Emissivity comparison of the same structure with different angles of incidence. e) Emissivity comparison of the same structure with different number of segments.

(Figure 4.10, b). For this structure, the dependencies of the emissivity from geometrical parameters are reported in figure (4.10). The increase of the thickness and the number of layers leads to a further improvement of the radiative properties of the structure (Figure 4.10, c-e). Finally, the absorptivity in near-IR and mid-IR is not strongly affected by the incident angle (Figure 4.10,d). However, the emissivity of real structures is spectral and directional dependent,  $\epsilon(\lambda, \theta)$ .

The structures studied in the paper of M.A. Kecebas *et al.* allow to obtain an emissivity very close to the ideal case. They are examined to give some guidelines for the design of radiative coolers. The optimization of these photonic structures requires an enormous computational load due to the large number of parameters that have to be considered, as reported in the paper of Raman *et al.*[25].

#### 4.2.3.2 Solar cell performance

Here, the impact on the solar cell of multilayer radiative cooler is evaluated and compared to the results previously obtained. To this scope, the thermal model presented in this chapter is employed using as emissivity the one of the structure

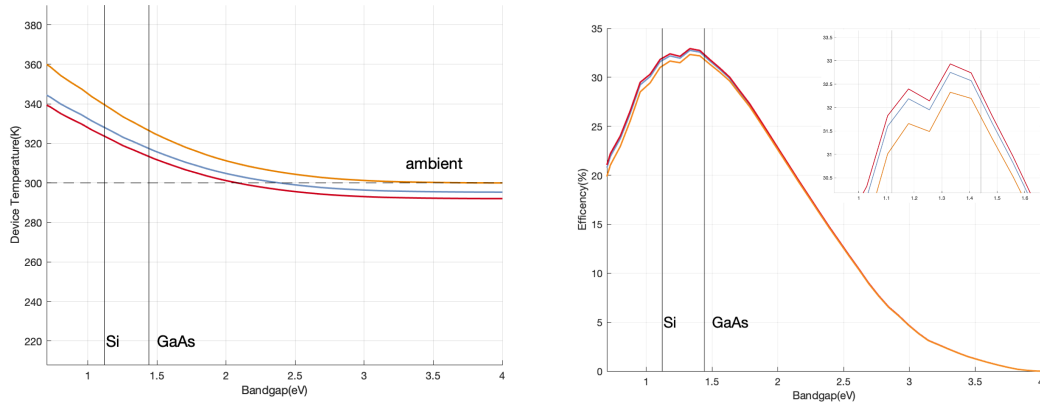


Figure 4.11: Left: Comparison between the temperature of different devices. Right: Comparison between the efficiency of different devices. (red: solar cell with ideal radiative cooler. blue: solar cell with multilayer radiative cooler. yellow: solar cell.)

in figure (4.10, a). Since the emissivity of the photonic structure is very high in the atmospheric transparency window, the temperatures reached by the solar cell with the *real* radiative cooler are close to the ideal case (Figure 4.11). The difference between the two temperatures is about 4.5 K. This leads to an efficiency decreases of 0.2%. However, as one can see in right figure (4.11), it is remarkably higher compared to the solar cell case.

# Conclusions

The enormous potential in multiple sustainable applications of passive day-time radiative cooling could significantly contribute to the reduction of global energy consumption and pave the way to a more green economy. Hence, the wide interest from both fundamental and applied sciences on this technology has led to a large production of scientific papers. All of these researches highlight the difficulties to construct cost-effective materials. In this context, the EU-funded Miracle project aims to develop and test a cheap and scalable photonic meta-concrete (PMC) with radiative cooling ability. This material will contribute to the construction of nearly zero-energy buildings (NZEB), but the employment of the PMC can be expanded to multiple fields such as air-conditioning systems and solar cell technology. The goal of the PoliTO team involved in this project is to study the employment of this material to tackle the reduction of solar cell efficiency due to the increase of temperature.

In this thesis, the physical mechanisms behind the passive radiative cooling technique and its application as a heat sink to increase the efficiency of a solar cell is examined and discussed. To do this, a state-of-art electromagnetic-thermal model was employed, taking into account only the radiative recombination process in the solar cell. This approach leads to an overestimation of the conversion efficiency and its temperature dependence. The model was tested through comparison with results in scientific literature, showing accuracy and versatility. Although the solar cell characterization, the obtained results are encouraging. Indeed, a silicon solar cell coupled with a radiative cooler in typical operating conditions shows an efficiency increase of 0.72% in the case of an ideal selective emitter, and 0.52% in the case of a realistic structure. It is a significant achievement considering the application of this technology on large scale. Indeed, this technique can be used to passively cool concentrated and non-concentrated PV systems, and in combination with other cooling mechanisms to further improve the energy production and the lifespan of solar cells. Furthermore, it reaches the maximum performance as a cooler in the space application, where the dominant heat transfer mechanisms is the radiative one.

More concrete and remarkable evaluations can be obtained employing a finite-difference-based thermal simulator for the estimation of non-radiative heat transfer mechanisms, and by considering the non-radiative recombination processes that

---

affect the solar cell performance, such as Auger. Finally, the electromagnetic and thermal model can be utilised as a useful tool in the research of new multilayer materials with radiative cooling capability for any kind of applications.

At the end of this thesis, the hope is that the interest in this new kind of technology will grow up in the coming years in order to improve the global energy consumption and production contributing to a greener future.

# Bibliography

- [1] IEA. Electricity market report - july 2021. *IEA, Paris*, July 2021. <https://www.iea.org/reports/electricity-market-report-july-2021>.
- [2] EIA. International energy outlook 2021. *U.S. Energy Information Administration*, 2021.
- [3] IEA. World energy outlook 2020. *IEA, Paris*, July 2021. <https://www.iea.org/reports/world-energy-outlook-2020>.
- [4] Wikipedia. Air mass (solar energy), cited October 2021. [https://en.wikipedia.org/wiki/Air\\_mass\\_\(solar\\_energy\)](https://en.wikipedia.org/wiki/Air_mass_(solar_energy)).
- [5] Natiolan Renewable Energy Laboratory. 2000 astm standard extraterrestrial spectrum reference e-490-00, 2000. <https://www.nrel.gov/grid/solar-resource/spectra-astm-e490.html>.
- [6] Natiolan Renewable Energy Laboratory. Reference air mass 1.5 spectra, 2003. <https://www.nrel.gov/grid/solar-resource/spectra-am1.5.html>.
- [7] C.B.Honsberg and S.G.Bowden. Photovoltaics education website, 2019. <https://www.pveducation.org/pvc/drom/properties-of-sunlight/solar-radiation-outside-the-earths-atmosphere>.
- [8] O. Isabella R. A. C. M. M. Van Swaaij A. H. M. Smets, K. Jager and M. Zeman. *Solar Energy - The physics and engineering of photovoltaic conversion, technologies and systems*. UIT Cambridge, 1 edition, February 2016.
- [9] P. J.Verlinden. *Chapter IC-5 - High-Efficiency Back-Contact Silicon Solar Cells for One-Sun and Concentrator Applications*. Elsevier, 2013.
- [10] W. Shockley and H. J. Queisser. Detailed balance limit of efficiency of pn junction solar cells. *Journal of Applied Physics* 32, 510, 1961.
- [11] A. Marti and G. L. Araujo. Limiting efficiencies for photovoltaic energy conversion in multigap systems. *Solar Energy Materials and Solar Cells, Vol. 43, Issue 2*, 1996.
- [12] S. Ruhle. Tabulated values of the shockley-queisser limit for single junction solar cells. *Solar Energy* 130, pages 139–47, 2016.
- [13] W. van Roosbroeck and W. Shockley. Photon-radiative recombination of electrons and holes in germanium. *Phys. Rev.*, 94:1558–1560, Jun 1954.
- [14] L. C. Hirst and N. J. Ekins-Daukes. Fundamental losses in solar cells. *Wiley Online Library*, August 2010.
- [15] R. V. Martin O. Dupre and A. Green. *Thermal Behavior of Photovoltaic*

- Devices*. Springer, 2017.
- [16] P. Würfel. *Physics of solar cells: from basic principles to advanced concepts*. Wiley, 2009.
- [17] E. Skoplaki and J. Palyvos. Prediction of building integrated photovoltaic cell temperatures. *Sol. Energy* 83, 2009.
- [18] J. R. G. Ross. Flat-plate photovoltaic array design optimization. *14th IEEE Conference on Photovoltaic Specialists Conference*, page 1126â1132, 1980.
- [19] J. R. G. Ross and M. I. Smokler. *Electricity from photovoltaic solar cells: Flat-Plate Solar Array Project Final Report*. <http://authors.library.caltech.edu/15040/1/JPLPub86-31volVI.pdf>, 1986.
- [20] R. Vaillon O. Dupre and M.A. Green. *A Thermal Model for the Design of Photovoltaic Devices*. In: *Thermal Behavior of Photovoltaic Devices*. Springer, Cham., 2017.
- [21] matprop.ru. Si - silicon. <http://www.ioffe.ru/SVA/NSM/Semicond/Si/bandstr.html#Temperature>.
- [22] E. Radziemska. The effect of temperature on the power drop in crystalline silicon solar cells. *Renewable Energy, Vol. 28, Issue 1*, 2003.
- [23] D. Otth and R. E. Ross Jr. Assessing photovoltaic module degradation and lifetime from long term environmental tests. *Proceedings of the 1983 Institute of Environmental Sciences 29th Annual Meeting, Los Angeles, CA*, April 1983.
- [24] P. Dwivedi K. Sudhakar A. Soni E. Solomin and I. Kirpichnikova. Advanced cooling techniques of p.v. modules: A state of art. *Elsevier Ltd.*, June 2020.
- [25] A. P. Raman M. A. Anoma L. Zhu E. Rephaeli and S. Fan. Passive radiative cooling below ambient air temperature under direct sunlight. *Nature* 515, 2014.
- [26] K. X. Wang M.A. Anoma L. Zhu, A. P. Raman and S. Fan. Radiative cooling of solar cells. *Optica Vol.1, No. 1*, 2014.
- [27] Y. Shi K. Chen L. Zhu W. Li and S. Fan. A comprehensive photonic approach for solar cell cooling. *ACS Photonics*, 2017.
- [28] I. Subedi N. J. Podraza I. M. Slauch V. E. Ferry T. J. Silverman, M. G. Deceglie and I. Repins. Reducing operating temperature in photovoltaic modules. *IEEE J. Photovoltaics*, 2018.
- [29] Z. Wang D. Kortge J. Zhu Z. Zhou H. Torsina C. Lee and P. Bermel. Lightweight, passive radiative cooling to enhance concentrating photovoltaics. *Joule* 4, 2020.
- [30] M. Planck. *The theory of heat radiation*. P. Blakiston's son and Co, 1 edition,

- 1914.
- [31] J. R. Howell R. Siegel and M. Pinar Menguc. *Thermal Radiation Heat Transfer; Volume 1*. Taylor Francis Group, 4 edition, 2002.
- [32] M. Born and E. Wolf. *Principles of Optics: Electromagnetic Theory of Propagation, Interference and Diffraction of Light*. Pergamon Press, 5 edition, 1974.
- [33] R. Orta. Passive optical components: Lecture notes. Politecnico di Torino, 2017.
- [34] C. Balaji. *Essentials of Radiation Heat Transfer*. Ane Books Pvt. Ltd., 1 edition, 2014.
- [35] Y. Zhai S. Xu Gang Tan X. Yin D. Zhao, A. Aili and R. Yang. Radiative sky cooling: Fundamental principles, materials, and applications. *Appl. Phys. Rev.* 6, April 16, 2019.
- [36] Gemini Observatory. Ir transmission spectra, 2003. <https://www.gemini.edu/observing/telescopes-and-sites/sites#Transmission>.
- [37] Z. Zhiguang L. Yu-wen, E. L. Schlenker and P. Bermel. Radiative cooling experiment, 2017. [Online]. Available: <https://nanohub.org/resources/radcool>.
- [38] L. Yu wen E. L. Schlenker Z. Zhiguang and P. Bermel. Radcool: a web-enabled simulation tool for radiative cooling. *The Summer Undergraduate Research Fellowship (SURF) Symposium*, August 3, 2017.
- [39] C. G. Granqvist and A. Hjortsberg. Radiative cooling to low temperatures: General considerations and application to selectively emitting sio films. *Appl. Phys.* 52, 1981.
- [40] S. Jeon and J. Shin. Ideal spectral emissivity for radiative cooling of earth-bound objects. *Sci. Rep.*, vol. 10, p. 13038, 2020.
- [41] N. M. Ravindra S. Abedrabbo W. Chen F. M. Tong A. K. Nanda and A. C. Speranza. Temperature-dependent emissivity of silicon-related materials and structures. *IEEE TRANSACTIONS ON SEMICONDUCTOR MANUFACTURING*, VOL. 11, NO. 1, February 1998.
- [42] T. S. Safi and J. N. Munday. Improving photovoltaic performance through radiative cooling in both terrestrial and extraterrestrial environments. *Opt. Express* 23, 2015.
- [43] G. Kenanakis E. N. Economou S. Tzortzakis G. Perrakis, A. C. Tasolamprou and M. Kafesaki. Passive radiative cooling for the temperature and efficiency control of photovoltaics. *OSA Technical Digest*, 2021.
- [44] Steve Graham. Remote sensing. *NASA earth observatory*, Sept. 1999. <http>

- s://earthobservatory.nasa.gov/features/RemoteSensing/remote\_04.php.
- [45] T. T. Chow. Performance analysis of photovoltaic-thermal collector by explicit dynamic model. *Solar Energy* 75, 2003.
- [46] Global wind atlas. <https://globalwindatlas.info/a>.
- [47] S. Bailey and R. Raffaele. Space solar cells and arrays, in handbook of photovoltaic science and engineering (a. luque and s. hegedus). *John Wiley and Sons*, 2005.
- [48] A. Kosar M. A. Kecebas, M. P. Menguc and K. Sendur. Passive radiative cooling design with broadband optical thin-film filters. *Journal of Quantitative Spectroscopy Radiative Transfer*, 2017.
- [49] O. Fedosenko S. Machulik A. Aleksandrova G. Monastyrskyi Y. Flores J. Kischkat Sven Peters, B. Gruska M. Semtsiv M. Chashnikova M. Klinkmuller and W. T. Masselink. Mid-infrared optical properties of thin films of aluminum oxide, titanium dioxide, silicon dioxide, aluminum nitride, and silicon nitride. *Appl. Opt.* 51, 2012.
- [50] M. L. Sundheimer E. Tucker G. D. Boreman M. B. Raschke H. U. Yang, J. D'Archangel. Optical dielectric function of silver. *Phys. Rev. B*91,, 2015.